5-2013

LASER-ASSISTED PRINTING OF ALGINATE AND CELLULAR TUBES

Jingyuan Yan
Clemson University, jingyuy@clemson.edu

LASER-ASSISTED PRINTING OF ALGINATE AND CELLULAR TUBES

A Thesis
Presented to
the Graduate School of
Clemson University

In Partial Fulfillment
of the Requirements for the Degree
Master of Science
Mechanical Engineering

---

by
Jingyuan Yan
May 2013

Accepted by:
Dr. Yong Huang, Committee Chair
Dr. Richard Miller
Dr. Rui Qiao

ABSTRACT

Laser-assisted printing such as laser-induced forward transfer (LIFT) has found increasing biofabrication applications as an orifice-free cell/organ printing approach. Unfortunately, there have been very few studies on its efficacy of three-dimensional (3D) printing performance. In addition, the effects of printing parameters on jet/droplet formation during the printing of Newtonian and non-Newtonian fluids are lacking. Therefore, it is important to investigate its printing process and quality. The resulting knowledge will help to better control the resulting printing quality and feature resolution.

The objective of this study is to investigate the feasibility of laser-assisted 3D printing process and its applicability in making non-cellular and cellular tubes. To better understand the printing process, the effects of fluid properties and operating conditions on the jet/droplet formation process is studied using time-resolved imaging analysis during LIFT of glycerol and sodium alginate (NaAlg) solutions. Operating diagrams regarding different jetting dynamics are constructed. In addition, the effects of NaAlg concentration and operating conditions on the printing quality during laser-assisted printing of alginate annular constructs (short tubes) with a nominal diameter of 3 mm has been studied.

It is found in this study that a well-defined jet forms only under certain combinations of glycerol/NaAlg concentration and laser fluence. The inverse of

Ohnesorge number is used to characterize the jettability (J) of glycerol solution. An operating diagram regarding J number and laser fluence is constructed for illustrating different printing regimes. An operating diagram is also constructed for NaAlg printing with respect to Deborah number and Reynolds number. It is found that in order to have jet contact-based printing, which is the preferred jetting regime, relatively large Deborah number and Reynolds number are favored.

It is also demonstrated that highly viscous materials such as alginate can be printed into well-defined long tubes and annular constructs. The tube wall thickness and tube outer diameter decrease with the NaAlg concentration, while they first increase, then decrease and finally increase again with the laser fluence. Alginate cellular tubes have also been printed with the post-printing cell viability of 60% immediately after printing and 80% after 24 hours of incubation.

To better understand the laser-assisted printing mechanism, more experimental and theoretical work on the entire printing process is expected. Prior to practical biomedical applications, printing of high concentration cell suspension to mimic the real tissue environment is desirable. Future work should also include mathematical models accounting for the entire printing process.

DEDICATION

This thesis is dedicated to my family for their love and support.

ACKNOWLEDGEMENTS

I wish to express my sincere thanks to my advisor, Professor Yong Huang, for his careful guidance, excellent suggestions and constructive criticism. His help and encouragement are deeply appreciated.

I would like to express my wholehearted gratitude to my other committee members, Dr. Richard Miller and Dr. Rui Qiao for their constructive review of this work and their suggestions.

I would like to thank Dr. Nicole Coutris and my group members who helped and supported me during the past two and half years at Clemson: Wenxuan Chai, Yafu Lin, Jun Yin, Leigh Herran, Changxue Xu, Fan Yang, Hemanth Gudapati, and Zhengyi Zhang.

I would also like to thank Jinxiang Zhou and Meng Zhang who gave me a lot of help in experiment measurements.

TABLE OF CONTENTS

Page

Table of Contents (Continued)

Page

Table of Contents (Continued)

Page

LIST OF TABLES

LIST OF FIGURES

List of Figures (Continued)

Figure Page

List of Figures (Continued)

Figure Page

List of Figures (Continued)

Figure Page

CHAPTER ONE

INTRODUCTION

1.1 Motivation and Background

Organ transplantation has been well-developed over past several decades, and it has saved the life of numerous patients with diseased organs. However, organ transplantation itself is limited by various hurdles such as pathogen transfer, immune rejection, high cost, and especially the donor shortage. For example, more than 112,000 people in the United States are awaiting organ transplantation in the year 2012. Besides, there is only one donor organ available for every 10 people on the organ transplant waiting list. In addition, there has been a major increase in the number of patients on transplant waiting list and a decrease of organ donors.

Fortunately, organ printing, an additive manufacturing technique-based approach, has emerged as a promising technological solution to tackle some of these hurdles. As envisioned, three-dimensional (3D) scaffold-free tissue or organ constructs will be fabricated [Mironov2009] [Wilson2003] [Riggs2011] [Wüst2011] in a layer-by-layer fashion using patient's cells based on the computer-aided model of patient-specific organs (Fig. 1.1).

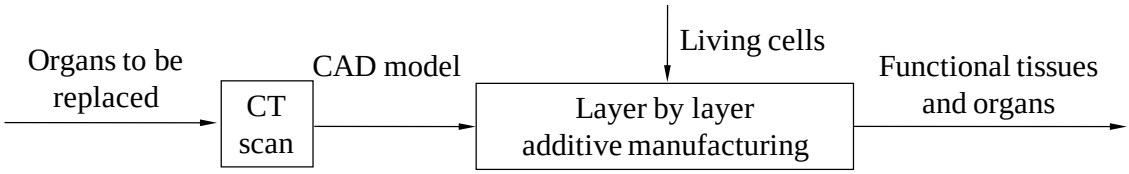

Fig. 1.1 Flow chart of organ printing

Fig. 1.2 shows an envisioned process of blood vessel printing. Annular structures consisting of cells from patients are printed layer by layer under the assistance of biopaper, which is a bio-compatible gel, or hydrogel that mimics the normal cell environment. The final product is made after further tissue fusion and tissue maturation. The challenges relating the LIFT technology and perspective practical organ printing rest in the following issues: (1) how to print 3D tissue constructs automatically and efficiently using LIFT; and (2) how to evaluate, model and quantify the LIFT-induced cell damage. Cell injury is unavoidable in bioprinting processes. Cell injury is sometimes reversible up to a certain point; however, exposure of a cell to a high magnitude and/or lasting external stress may cause irreversible cell injury even cell death.

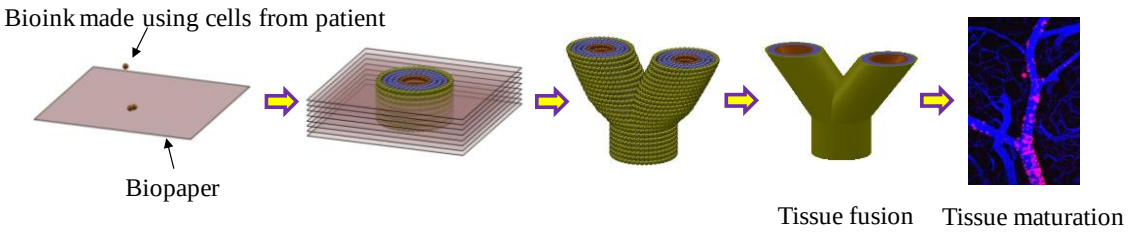

Fig. 1.2 Schematic of envisioned fabrication of vascular trees

Homogeneous cells have been conventionally seeded using soft lithography, dipping, and microlitre syringe dispatching, to name a few. As a result, seeded cells are usually uniform and mostly in a two-dimensional (2D) form, which may not be sufficient for some controlled gradient and/or 3D cell applications.

As a promising alternative, cell direct writing or cell printing has emerged as a revolutionary advance in tissue engineering with great potential for use in the manufacture of arbitrary cell patterning as well as heterogeneous 2D or 3D living scaffolds [Lewis2004] [Barbulovic-Nad2006] [Ringeisen2006]. Among all the possible patterns or structures, the most promising way is to directly print a 3D construct without any scaffold. Different 3D scaffold-free heterogeneous structures can be fabricated using various 3D additive printing technologies, for example, jet contact-based laser printing [Riggs2011] and inkjet printing [Boland2007]. During 3D additive printing, constituent materials of structure or their precursors are dispensed three dimensionally to construct the 3D product layer-by-layer based on computer-aided models. Currently, 3D additive printing and its variations have been implemented to create various 3D patterns and structures and found numerous engineering and biomedical applications [Riggs2011] [Wohlers2001] [Boland2006]. One of its most exciting applications is to fabricate human tissues and organs suitable for regeneration, repair and replacement of damaged, injured or lost cells [Mironov2009], which is generally called cell/organ printing or bioprinting.

Generally, 3D additive printing-based organ printing or 3D organ printing can be implemented using orifice-based and orifice-free approaches. As the widely used orifice-based fabrication approach, inkjetting has been applied to fabricate various biological patterns or constructs such as alginate tubes [Nishiyama2009] [Xu2012]. However, orifice-based printing may experience a great difficulty in printing viscous biological materials such as alginate, which may clog the nozzle during printing. For example, only NaAlg with concentrations lower than 2% is recommended for inkjetting [Norman2006] [Herran2012a] [Herran2012b]. As such, orifice-free techniques should be developed for the printing of viscous materials, including PEG, biomaterials and biological materials, which are common constituents of many biological constructs. Fortunately, laser-assisted printing/direct writing, an orifice-free printing approach developed based on LIFT, has been investigated to print and pattern different materials including biomaterials and biological materials [Riggs2011] [Barron2005] [Lin2009a] [Koch2010] [Schiele2010] [Lin2011] [Barron2004] [Ringeisen2004] [Lin2010]. LIFT serves as a complementary clogging-free bioprinting technique to inkjetting for some viscous printing applications [Lin2011].

In order to understand the printing mechanism of LIFT technology, the entire printing process should be monitored and the favored printing conditions are to be determined. The minimum feature size for LIFT and thus the proposed laser-assisted

printing is of great interest for microfabrication, and it is closely related to the jet and droplet formation process [Lin2009b]. Ideally, monodispersed droplets are desired during LIFT. As such, it is important to understand and further model the jet and droplet formation process and the droplet landing/spreading process under different LIFT operating conditions when different electronic or biological materials are used. This will allow better control of the resulting printing quality and feature resolution.

1.2 Current Research State

The laser-assisted printing process includes some critical steps: bubble formation, jet/droplet formation, landing and/or jet breakup. During LIFT, a laser pulse is focused perpendicularly through the backside of a quartz support-based ribbon, which consists of an optically transparent quartz disk and a coated material (ribbon coating and/or a layer of energy absorbing material) to be transferred. The ribbon coating is then locally heated by the laser beam, immediately generating a small vapor pocket/bubble at the interface of the quartz disk and coating. The generated bubble then expands rapidly and ejects part of the coating material downwards, forming a jet/droplet for deposition [Lin2009b] [Guillemot2010b].

Previous study has been performed to investigate the relationship between the operating conditions especially laser fluence and the bubble or droplet size in LIFT. For

example, Brown et al. [Brown2010] discovered a strong dependence of the bubble size and shape on ribbon coating thickness, laser beam diameter and laser fluence, demonstrating a potential of optimization. Lin et al. [Lin2009b] found out that the formed bubble diameter increases with the laser fluence and the formed bubble diameter first decreases and then increases with the glycerol concentration. Moreover, at a given glycerol concentration, the droplet diameter is linearly dependent on the laser fluence, and the slope of this linear relationship between the droplet diameter and the laser fluence is dependent on the glycerol concentration. Colina et al. [Colina2006] concluded a linear relationship between the laser pulse energy and the droplet volume while Kattamis et al. [Kattamis2007] identified the linear relationship between the laser energy and the droplet diameter. The relationship between material properties and droplet size in LIFT has also been investigated by previous studies. For example, Lin et al. [Lin2009b] observed that the droplet diameter has no systematic relationship with the glycerol concentration. At a given laser fluence, the droplet diameter increases with the increase of glycerol concentration ratio until it reaches a transitional concentration ratio for the largest droplet. The droplet diameter would decrease with the increase of glycerol concentration ratio, once the glycerol concentration ratio is higher than the concentration ratio for the largest droplet. The concentration ratio for the largest droplet is a function of laser fluence, and it generally increases as the laser fluence increases. However, the effects of matrix material

properties and various operating conditions have not been systematically investigated thus far in LIFT applications.

Jet/droplet formation is an important step during fluid jet contact-based direct writing or printing, which determines the pattern uniformity and spatial accuracy. During orifice-based direct writing, fluid jets are first ejected from an orifice and then broken into droplets with, or without, satellite droplets [Herran2010] [Herran2012a]. The generated droplets are combined to form various structures in a controllable manner. During laser-assisted orifice-free direct writing such as LIFT, the material transfer and deposition can be due to either ejected droplets [Barron2005] [Young2002] or the contact between formed long, thin jet and the receiving substrate [Duocastella2008] [Serra2009] depending on the direct writing height and the material properties.

The jet formation mechanism in laser-assisted direct writing has been studied using time-resolved imaging analysis [Serra2009] [Duocastella2009] [Duocastella2010] [Unger2011]. Depending on the applied laser fluence, three distinct working regimes have been identified: sub-threshold (no material deposition), jetting (having well-defined jet formation), and plume (generating atomized droplets) [Lin2009b] [Young2002] [Duocastella2009] [Guillemot2010a]. The well-defined jet formation regime is generally desired for better direct writing. During this process, a bubble is first generated by absorbing the energy of the incident laser pulse, and then a needlelike jet is formed as the

bubble expands, and finally a long, thin jet is formed. In addition, some phenomena may accompany the formation of the well-defined jet. For example, the formation of a counter jet inside the ribbon coating [Duocastella2009], a bulgy structure due to the possible lateral collapse of jet [Unger2011], or droplets after jet breakup [Brown2010].

Jet morphology has been characterized in terms of the bubble size [Brown2010], jet diameter [Duocastella2009] [Unger2011], and jet breakup [Unger2011] [Brown2010]. Specifically, the effects of laser fluence on the jet morphology and jet velocity have been studied [Young2002] [Duocastella2009] [Unger2011] [Brown2011], and the jet and plume velocities were found to increase with the laser fluence [Young2002] [Duocastella2009]. In addition, the jet formation process has been evaluated under various operating conditions such as the sacrificial layer thickness [Brown2010], ribbon coating thickness [Duocastella2011a], direct writing height [Serra2009] [Duocastella2007], and laser beam dimensions [Brown2010] [Colina2006].

The jetting phenomena and printing mechanism can be also different depending on different experimental conditions. Unger et al. [Unger2011] printed 2% NaAlg using LIFT technique by applying 1.6 and 2.7 J/cm^2 laser fluences with direct writing height of 450 μm. The deposited droplet was formed by the contact of a jet with the receiving substrate. Duocastella et. al [Duocastella2011a] printed 50% glycerol solution with laser fluence of 4 J/cm^2 and direct writing height of 350 μm. Similarly, the deposition was jet

contact-based. An alternative mechanism was also observed by Duocastella et. al [Duocastella2011b] that droplet was formed by bubble contact, with the laser fluence of 12 J/cm^2 and direct writing height of 250 μm. However, the study on material properties and operating conditions are lacking, and the study on jetting and deposition regimes of viscoelastic material is lacking.

While it has been proved to be a viable technique in printing various cells such as yeast cells [Lin2009a], rat cardiac cells [Barron2004], mouse pluripotent embryonal carcinoma P19 cells [Ringeisen2004], human colon cancer cells [Lin2010], skin cells (NIH 3T3 fibroblast/HaCaT keratinocytes) [Koch2010], human osteosarcoma cells [Barron2004], and human mesenchymal stem cells (hMSC) [Koch2010], LIFT has been pioneered to print different biological patterns. For example, Koch *et al* [Koch2010] made a chess board pattern using fibroblasts (NIH 3T3) and keratinocytes (HaCaT); Gruene *et al* [Gruene2011] fabricated two-dimensional (2D) word and grid patterns using porcine bone marrow-derived mesenchymal stem cells; Catros *et al* [Catros2011] laser printed human osteoprogenitors (HOPs) into 2D and 3D annular patterns; and Koch *et al* [Koch2012] printed a 3D layered construct (homogeneous along the horizontal plane) based on the alternating layers of HaCaT keratinocytes dyed with different colors. However, laser-assisted printing has not been studied to fabricate 3D scaffold-free tubular constructs thus far. In the field of biofabrication, the fabrication of hollow cellular tubes

to mimic vascular structures have been widely recognized as not only the first logical step towards successful organ printing but also a critical indicator of the feasibility of the envisioned organ printing technology [Mironov2003].

However, the investigation about the effects of fluid properties as well as the operating conditions on the jet formation process is still largely elusive. In addition, few studies have focused on LIFT process of viscoelastic materials. For example, Unger et al. [Unger2011] carried a time-resolved imaging study on the jet formation process during LIFT of 2% NaAlg solution. They showed the entire printing process under two different laser fluences as well as the effects of the presence of a receiving substrate. It was demonstrated that higher impact velocities induced splashing of the droplet. Besides, the transfer duration is stabilized by the presence of a collector slide. The behavior of viscoelastic material has been investigated in inkjetting. Elasticity can accelerate the growth of capillary disturbances but prolongs the lifetime of a thinning thread before its eventual breakup. Moreover, because of the extended thread lifetime relative to the Newtonian case, a viscoelastic jet may remain intact for considerably longer periods of time, taking the form of a series of near-spherical beads connected by thin filaments. This phenomenon is called ‘beads-on-a-string’ (BOAS) [Morrison2010].

In this study, time resolved imaging analysis has been applied to investigate the individual and combined effects of fluid properties and laser fluence on the printing

process of glycerol solution, and to investigate the fluid properties and various operating conditions such as laser fluence, laser spot size and direct writing height on the printing process of NaAlg solution to have a comprehensive understanding of the LIFT technology.

1.3 Objective

The objective of this study is to study the feasibility of laser printing of alginate tubes and investigate the effects of NaAlg concentration and operating conditions such as the laser fluence and laser spot size on the printing quality. In order to better understand the printing mechanism and better control the printing process, time-resolved imaging analysis is carried to study the effects of fluid properties and operating conditions such as laser fluence, laser spot size and direct writing height on the jet/droplet formation process during laser-assisted printing of glycerol and NaAlg solutions. In this study, NaAlg and calcium chloride were used as the gel precursor and gel reactant solutions, respectively, for the making of alginate tubes due to their wide applications in the healthcare field. Cellular tube printing is expected following the printing of alginate tubes. This thesis serves a preliminary investigation towards 3D organ printing using LIFT technology. The relation among the chapters of this thesis is illustrated in Fig. 1.3.

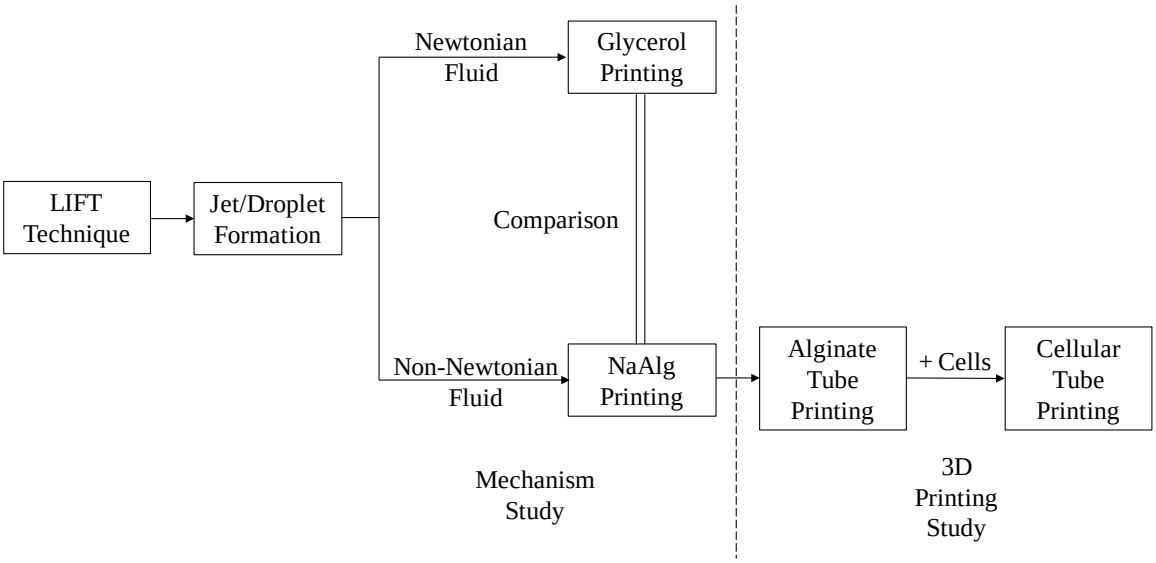

Fig. 1.3 Relation of each part of this thesis

The organization of this thesis is as follows:

In Chapter 1, the motivation and background of this work are first introduced. The current research state is then reviewed. Then the objective of this study is presented. Finally, the scope of this dissertation is provided.

In Chapter 2, the mechanism of printing is first discussed in general. Then experimental setups and material are given for the four main experiments in this thesis: imaging analysis of glycerol solution printing, imaging analysis of NaAlg solution printing, laser-assisted printing of alginate tubes, and laser-assisted printing of cellular tubes.

In Chapter 3, the printing process of glycerol solutions is studied by imaging

analysis. The effect of material properties and laser fluence and their combined effect are discussed then. According to the experimental results and analysis, an operating diagram regarding Jettability (*J* number) and laser fluence is presented.

In Chapter 4, imaging analysis is carried to study the printing process of NaAlg solutions. The effects of material properties and operating conditions such as laser fluence, laser spot size and direct writing height on the printing process is discussed in combination of the dimensionless numbers. Then, the different printing regimes are identified and studied. An operating diagram is constructed regarding Deborah number and Reynolds number to identify printing regimes. Finally, the printing process of Newtonian and viscoelastic materials are compared.

In Chapter 5, the experimental result for laser-assisted printing of alginate tubes is first given. Then the effects of NaAlg concentration and operating conditions on the printing quality, particularly the tube outer diameter and tube wall thickness, are discussed respectively. Finally, the laser-assisted printing result of cellular tubes is shown.

In Chapter 6, conclusions and future work of this thesis are summarized.

CHAPTER TWO

MECHANISM INTRODUCTION AND EXPERIMENTAL DESIGN

2.1 Mechanism Introduction

Matrix-assisted pulsed-laser evaporation direct-write (MAPLE DW), a type of modified LIFT technique, is of interest in the study of jet formation during laser-assisted direct writing. Regarding the MAPLE DW working mechanism, it is generally believed that it is the laser-material interaction-induced pressure that is responsible for material ejection and transfer. Such mechanism in converting laser pulse energy into pressure has also found other applications in laser shock peening [Fabbro1990] [Sollier2001], laser micro-dissection and laser pressure catapulting [Vogel2007], to name a few. The laser-induced pressure generation is generally attributed to plasma formation, rapid evaporation (including normal boiling and phase explosion), and thermoelastic effect (mainly thermal expansion-induced and no phase change involved) [Park1994] [Vogel2003].

The printing mechanism is shown in Fig. 2.1, the ultraviolet laser pulse is focused perpendicularly through the backside of a ribbon that consists of an optically transparent quartz disk with a coated thin film, known as the ribbon coating. The ribbon coating is locally heated and sublimed by the incident laser pulse, generating a small vapor

pocket/bubble at the interface between the ribbon coating and the quartz support. Because of rapid localized heating, the resulting bubble expands rapidly. The expansion of the bubble then helps eject the coating material beneath away from the ribbon onto the receiving substrate [Lin2009b]. In this way, the coating materials are transferred onto the receiving substrate to fabricate various patterns or structures.

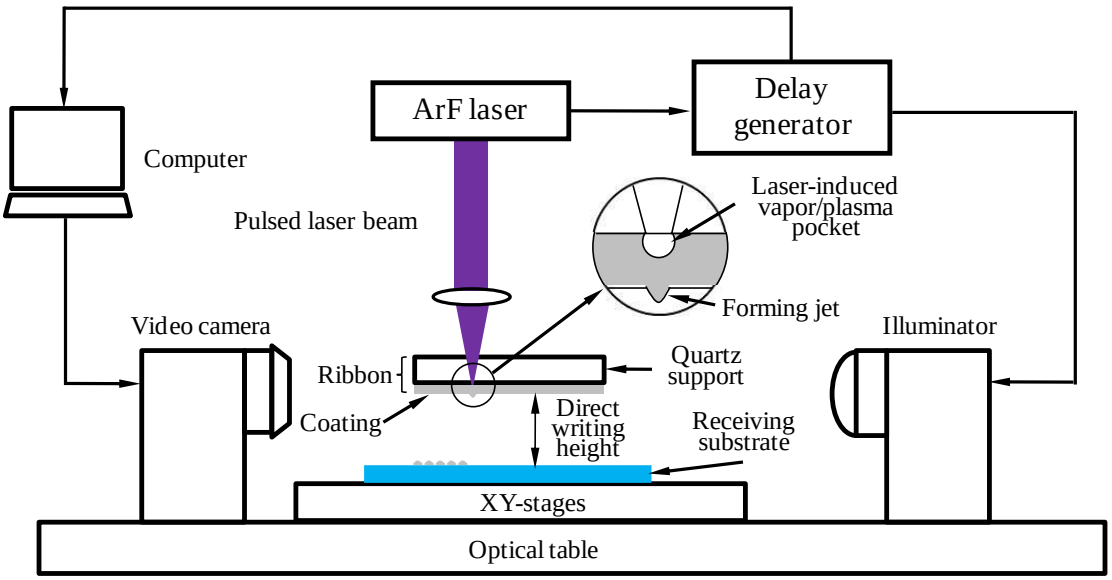

(a)

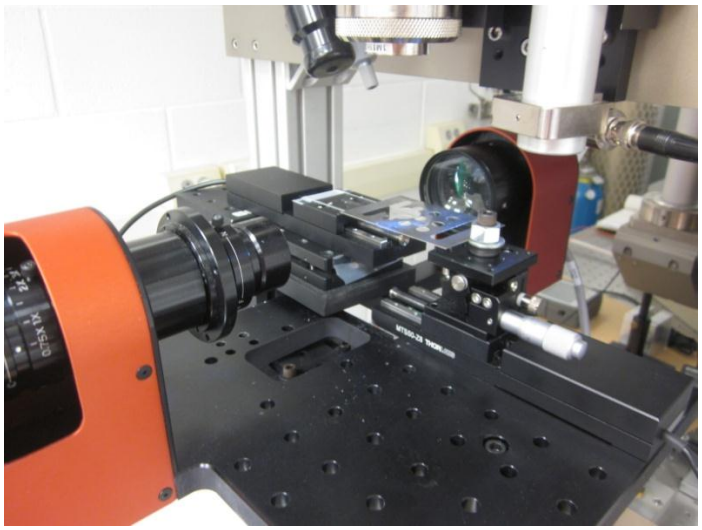

(b)

Fig. 2.1 Experimental setup consisting of the MAPLE DW apparatus and an imaging system: (a) schematics, and (b) apparatus

2.2 Experimental Setup and Materials

2.2.1 Newtonian Fluid Printing

In this study, glycerol-water solution is transferred using MAPLE DW. The glycerol solution has been tested as Newtonian fluid because of its relevance to biomedical applications [Lin2009b].

The MAPLE DW setup herein included an ArF excimer laser (Coherent ExciStar, 193 nm, 12 ns full-width half-maximum) with a laser spot size of 150 μm in diameter and a repetition rate of 2 Hz. A quartz optical flat disk (Edmund optics, Barrington, NJ) with 85% transmittance for 193 nm wavelength beams was used to make the ribbon, which was attached to a specially designed fixture. The levels of applied laser energy were 0.15, 0.20, 0.25, and 0.30 mJ, and the actual laser fluence during direct writing was determined based on the averaged measurements using a FieldMax laser power/energy meter (Coherent, Santa Clara, CA). The measured laser fluence level varied slightly every time under the same operating conditions due to the laser output instability. The laser fluences measured after 15% loss due to the quartz disk were 717 ± 45, 957 ± 35, 1183 ± 67, and 1433 ± 77 mJ/cm^2.

The jet formation process and jet velocity were monitored and estimated using the JetXpert imaging system (ImageXpert Inc., Nashua, NH). The light strobe was triggered by the control pulse from the laser, and a single image frame was acquired for each laser

pulse using an integration time of 2 μs. The system was set up at the grazing incidence with respect to the coating surface without the receiving substrate in the camera scope. Fifty laser pulses were emitted each time for a given laser fluence and glycerol concentration combination. The jet formation process was captured by the imaging system one frame per second, triggered by the output control signal of the laser, and a single image frame was acquired for each laser pulse as in other studies [Duocastella2009] [Unger2011] [Brown2010] [Kaur2009]. The jet velocity was estimated based on the spatial position difference of jet front of two sequential imaging frames of the jetting process.

Glycerol (Acros Organics, Fair Lawn, NJ, 99% pure) and de-ionized water were used to make the glycerol-water solution with different glycerol concentrations (v/v): 15%, 25%, 35%, 50%, 65%, 75%, 85%, and 99%. The matrix was prepared at a thickness of 100 μm by blade coating 15 μl glycerol-water solution onto a 1.5 cm (length) × 1 cm (width) × 100 μm (depth) plastic frame on the quartz disk.

2.2.2 Non-Newtonian Fluid Printing

Alginate, particularly, sodium alginate, has been used as a constituent of bioink in bioprinting [Nishiyama2009] [Khalil2005] [Phamduy2012]. Alginate hydrogels are often favored due to their resemblance of natural extracellular matrix (ECM) [Tan2007]. While

alginate is not an ideal material for living tissue construction, it is a good hydrogel material for proof-of-concept studies [Xu2012]. As such, NaAlg (Sigma-Aldrich, St. Louis, MO) and deionized water were used to prepare the NaAlg solution with different concentrations: 2%, 4% and 6% (w/v). High concentration alginate solutions were used in order to simulate application scenarios during the printing of viscous hydrogel materials.

Glycerol solution was used as a comparable Newtonian fluid to the viscoelastic fluid. Glycerol (Acros Organics, Fair Lawn, NJ, 99% pure) and de-ionized water were used to make the glycerol-water solution with glycerol concentrations of 85% (v/v), which has the same zero-shear viscosity of 2% NaAlg. The material properties of the Newtonian ink and viscoelastic ink are shown in Table 1, in which the surface tension was measured using a contact angle measuring instrument DSA10-MK2 (Krüss GmbH, Hamburg, Germany). The viscosity was measured using cup-and-bob rheometer (ARES, TA Instrument, New Castle, DE).

Table 1 Material properties of NaAlg and glycerol

Material	Concentration (%)	Density ρ (g/cm^3)	Surface tension σ (mN/m)	Viscosity η_0 (mPa s)
NaAlg	2	1.02	45.64	132.57
	4	1.04	44.41	885.82
	6	1.06	43.71	3123.56
Glycerol	85	1.23	64.90	127.19

In this experiment design, NaAlg and glycerol solutions were used as printing inks which are transferred respectively with MAPLE DW. The apparatus and experimental setup have been discussed above. The entire printing process is defined as from the jet formation to jet ending when there is no droplet within the scope. In this study, a series of pictures were taken every 100 μs with 10 μs of delay between every two sequential imaging frames. If the printing did not finish, then another 100 μs were examined in the same way. The jet velocity was estimated based on the spatial position difference of jet front of two sequential imaging frames of the printing process.

The laser fluences measured after 15% loss due to the quartz disk were 686 ± 19, 861 ± 20, 1021 ± 22, 1196 ± 29, and 1380 ± 34 mJ/cm^2. Two laser spot sizes (150 and 50

μm) were used in this study by applying two different copper masks on the beam path. The direct writing height is determined as the distance between the ribbon coating and receiving substrate (Fig. 2.1), and it was varied as 0.5, 1, 1.4 and 1.8 mm in this study.

2.2.3 Alginate Tube Printing

Materials

Alginate, particularly, sodium alginate, has been used as a constituent of bioink in bioprinting [Nishiyama2009] [Khalil2005] [Phamduy2012]. As such, NaAlg (product number W201502, Sigma-Aldrich, St. Louis, MO), which has a molecular weight range of 20–40 kDa, and deionized water were used to prepare the NaAlg solution with different concentrations: 1%, 2%, 4%, 6%, and 8% (w/v). High concentration alginate solutions were used in order to simulate application scenarios during the printing of viscous hydrogel materials. Calcium chloride dihydrate (Sigma-Aldrich, St. Louis, MO), a cross-linking agent, was used as a source of calcium ions to initiate gelation once the NaAlg was merged into a calcium chloride bath. It should be noted that while alginate is not an ideal material for living tissue construction, it is a good hydrogel material for proof-of-concept studies. If not specified, the calcium chloride concentration was 2% (w/v) in this section.

Experimental Apparatus and Fabrication Mechanism

Matrix-assisted pulsed-laser evaporation direct-write (MAPLE DW), a typical LIFT practice [Schiele2010] [Lin2009b], has been of particular interest in this study as the laser-assisted printing technique. As shown in Fig. 2.2, part of the alginate solution, which was coated on the bottom side of the quartz disk-based ribbon, was ejected due to the laser pulse-induced high pressure bubble [Lin2009b] and deposited on the receiving platform inside the calcium chloride container. The laser printing setup contained a 193nm, 12 ns (full-width half-maximum) ArF excimer laser (Coherent ExciStar, Santa Clara, CA) and an optical beam delivery system. The laser spot size was controlled at 150 μm in diameter, and the actual laser fluence was measured using a Coherent FieldMax power/energy meter (Coherent, Portland, OR). The laser repetition rate was set at 10 Hz. Quartz disk (Edmund optics, Barrington, NJ) with 85% transmittance for 193 nm wavelength laser beams was used to make the ribbon, which had the alginate coating on the bottom side. The NaAlg solution was coated using a film applicator (MTI, Richmond, CA), resulting the ribbon coating with a thickness of 100 μm.

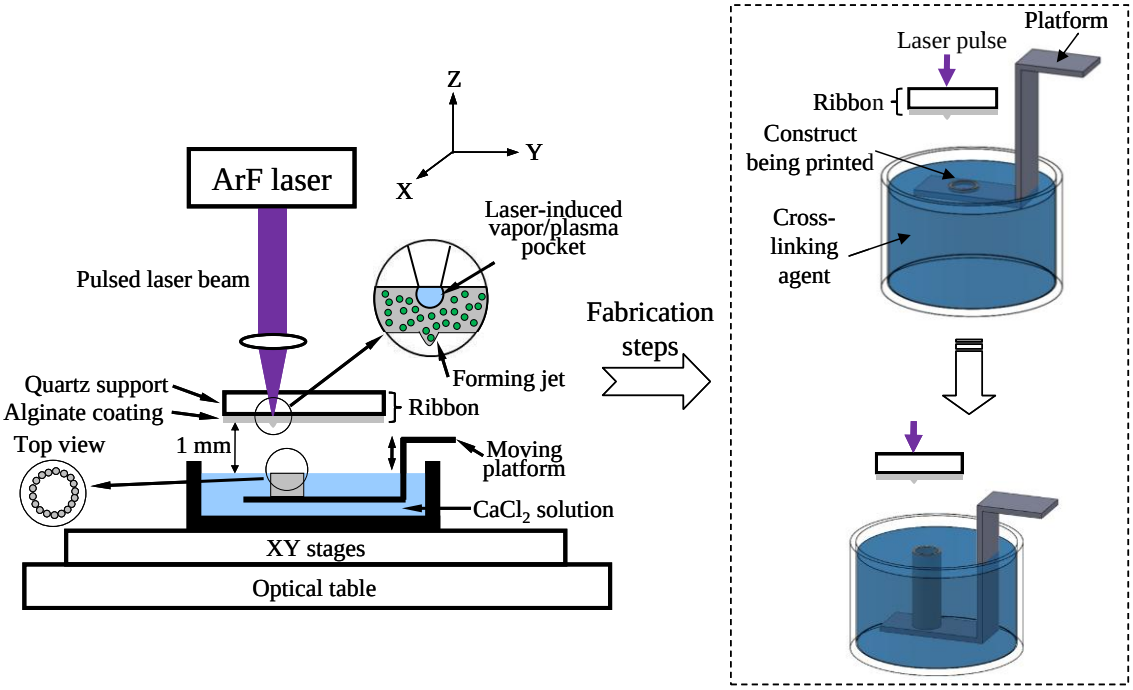

(a)

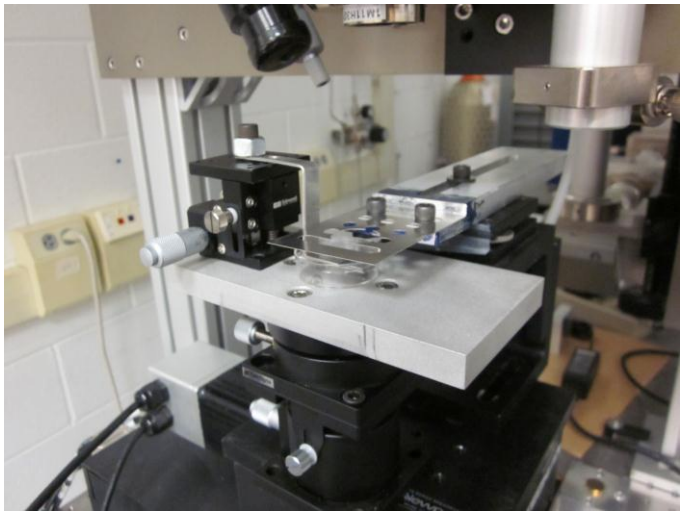

(b)

Fig. 2.2 Laser-assisted alginate tube printing experimental setup and fabrication steps (a) schematics, and (b) apparatus

During the printing process, the landing location for alginate droplets being deposited was the newly printed top layer of the construct being printed. The direct writing height, the distance between the ribbon and the liquid level, was set at 1 mm to optimize the printing quality in terms of the feature size of deposited feature (tube wall). The top layer was controlled around 0.5 mm above the liquid level to avoid possible contact between the ribbon coating and the calcium chloride solution, resulting in a 0.5 mm gap between the ribbon coating and the top layer. Once deposited, the platform moved downwards to submerge into the calcium chloride solution to fully gelatinize the newly deposited alginate droplet contact-based layer. Subsequently, this newly deposited layer was raised 0.5 mm above the liquid level before continuing the subsequent round of printing, thus, the platform moved down around 25 μm between any two consecutive printing positions, meaning a layer thickness of 25 μm. This process repeated until a construct was made. In addition, the jet formation process was also monitored using JetXpert (ImageXpert Inc., Nashua, NH).

The relative motion between the ribbon and the receiving container was controlled using XY translational stages (Aerotech, Pittsburgh, PA). The laser beam horizontal traveling speed was set at 100 mm/min, resulting in a 167 μm spatial distance between two consecutive pulses. The downward motion of the platform, on which the construct was printed, was precisely controlled using a Z axis stage (Thorlabs, Newton,

NJ). The post-printing measurements were conducted immediately after the making of alginate tubes, and the residual liquid inside tubes was removed out using a pipette. For each tube, four measurements were conducted equidistantly along the circumferential direction to get the averaged wall thickness and tube outer diameter. Under each fabrication condition, three tubes were made, and the reported wall thickness and tube diameter were the averaged values of those of three tubes.

Design of Experiments

In this study, some long, straight alginate tubes (6 mm in height, 240 layers) were fabricated first to prove the feasibility in making such tubes. Then a parametric study was conducted to appreciate the effects of material properties and operating conditions on the printing quality by printing annular constructs or short tubes (around 1 mm in height, 20 layers). It should be pointed out that the construct height is not proportional to the number of layers due to the increasing wall thickness as the height increases. The printing quality herein is evaluated based on the wall thickness and diameter of printed tubes, and the annular constructs (short tubes) are discussed as tubes for convenience in the following sections. For all experiments, the concentration of calcium chloride solution was 2%. For all tubes, the nominal tube diameter, which is the diameter defined by the center of laser beam spot, was controlled at 3 mm.

The parametric study was implemented in three different setups to appreciate the effects of NaAlg concentration, laser fluence, and laser spot size on the printing quality. The first setup was to study the effect of NaAlg concentration on the printing quality, and annular constructs were printed using 2%, 4%, 6% and 8% NaAlg solutions while keeping the laser fluence at 1437 ± 28 mJ/cm^2. The second setup was to study the effect of laser fluence, and the laser fluence was varied as follows: 1149 ± 31 mJ/cm^2, 1437 ± 28 mJ/cm^2, 1698 ± 45 mJ/cm^2, 2009 ± 45 mJ/cm^2 and 2286 ± 45 mJ/cm^2 for each of 2%, 4%, 6% and 8% NaAlg solutions. The third setup was to study the effect of laser spot size, and a 50 μm (in diameter) spot size was studied in addition to the nominal spot size (150 μm) for 2%, 4%, 6% and 8% NaAlg solutions, respectively, under a laser fluence of 2286 ± 45 mJ/cm^2.

2.2.4 Cellular Tube Printing

The general experimental setup was similar as the one for laser-assisted printing of alginate tubes. For the printing of alginate tubes, bioink was used instead of NaAlg solution. The bioink was comprised of NaAlg solution and NIH3T3 cells to be transferred. Each time, 60 μl of the bioink was pipetted onto the quartz disk and was spread evenly to make a thick layer. The laser fluence was maintained at 1026 ± 27 mJ/cm^2. The laser spot size used was 150 μm in diameter and the pulse frequency was 20 Hz. The direct writing

height here was maintained at about 1.8 mm due to experimental apparatus constraint. In order to expedite the cellular tube fabrication process, the entire printing was automated in this experiment (Fig. 2.3). In addition, fewer cells would die before incubation using printing automation. During the printing process, the platform, the container, and the Z stage was moving with the XY stages at a speed of 200 mm/min and were relatively immobile. The feed speed of the ribbon was 1.5 mm/s, and the descend speed of the platform was 2.5 μm/s. The printed cellular tube was incubated for 24 hours and then cell viability was tested.

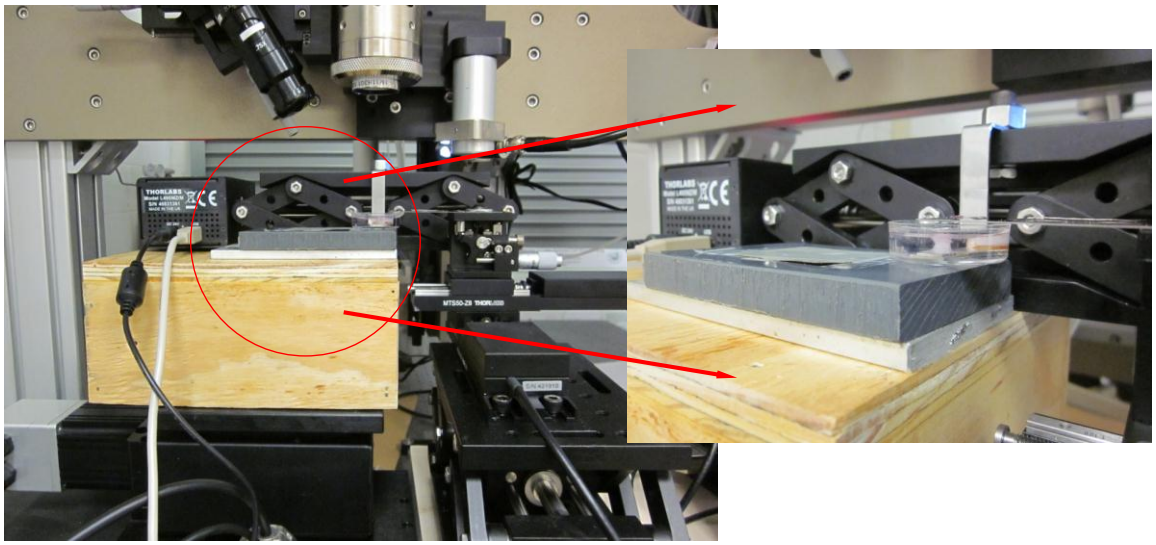

Fig. 2.3 Laser-assisted cellular tube printing apparatus

Bioink Preparation

The bioink was primarily comprised of NaAlg solution and NIH3T3 mouse fibroblast cells. The cells were cultured in DMEM (Sigma Aldrich, St. Louis, MO) supplemented with 10% Fetal Bovine Serum (FBS) (HyClone, Logan, UT) in a humidified 5% CO_2 incubator (VWR, Radnor, PA) at 37℃, and the culture medium was replaced every three days as required. Freshly confluent flasks of 3T3 fibroblasts were washed twice with Dulbecco's phosphate-buffered saline (PBS) (Cellgro, Manassas, VA), and incubated with 0.25% Trypsin/EDTA (Sigma Aldrich, St. Louis, MO) for 5 min at 37℃ to detach the cells from the culture flasks. Then the cell suspension was centrifuged at 1000 rpm for 5 minutes at room temperature, and the resulting pellet was resuspended in DMEM complete cell culture medium. The resuspended cells were adjusted to the cell concentration of 1×10^7 cells/ml. Then 4% NaAlg solution was mixed with NIH3T3 cells at a 50-50 percent volume ratio to obtain 2% (w/v) of bioink with 5×10^6 cells/ml.

Ribbon Preparation

Initially, the quartz disks were cleaned with an ultrasonic cleaner (Branson, Danbury, CT) and de-ionized water for five minutes. The quartz disks were then rinsed with 70% ethanol. Later, the quartz disks were washed with water and were air dried. Then the quartz disks were sterilized using an ultraviolet lamp for 15 minutes on the side

that was coated with bioink. 1 inch × 2 inches rectangular Quartz disks (Knight optical, Kent, UK) with 85% transmittance for 193 nm wavelength laser beams were used to make the ribbon, which had the bottom side coated with the bioink.

Evaluation of Cell Viability

The cell viability of the printed tubes was tested immediately after printing and after 24 hours of incubation respectively. The printed cellular tube was liquefied using 0.5 ml of 0.055 M sodium citrate solution. The tube was allowed to interact with sodium citrate for several minutes to complete liquefication. The resulting solution inside the centrifuge tube was then centrifuged for four minutes at 1000 rpm. Then, the supernatant sodium citrate solution was pipetted out, leaving cells with small amount of liquid at the bottom of the centrifuge tube.

The testing solution used for evaluating the cell viability was 0.4% trypan blue stain (Biowhittaker, Walkersville, MD). Post-transfer cell suspension and trypan blue dye were mixed at a 50-50 percent volume ratio to make a testing sample. The sample was pipetted onto a hemocytometer (Hausser Scientific, Horsham, PA) and then was viewed using an optical microscope. Fig. 2.4 shows a sample of live and dead cells under microscopic view. For the cells with intact cell membrane, the blue indicator turned bright and colorless in the presence of active enzymes, thus indicating live cells. For the

cells with permeable cell membrane, the blue stain remained inside the cells, indicating dead cells. Thereafter, the live and the dead cells were counted under the microscope.

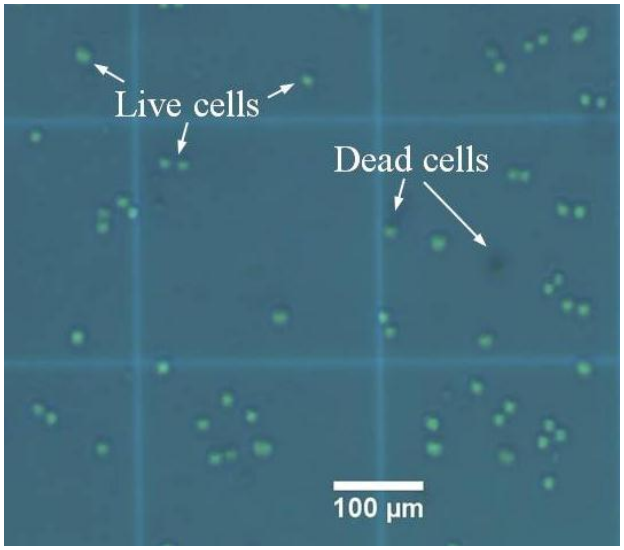

Fig. 2.4 Post-transfer NIH3T3 cells stained with trypan blue

The control cell samples were tested using unprinted cell-NaAlg mixture. The control sample for no incubation was tested in the same way, while for the incubation control, the procedure is as follows. After 24 hours of incubation, the control cells were detached by trypsinization, prior to evaluation of the viability. The trypsinization process can be briefly described as, first, DMEM medium was pipetted out into a centrifuge tube from the Petri dish. Second, cells in the Petri dish were washed with the DPBS solution and third, 0.5 ml of 0.25% Trypsin-EDTA solution was added to the culture dish. Fourth,

the cells in the Petri dish together with the Trypsin-EDTA solution were incubated for 3-5 minutes. Fifth, the cells and the Trypsin-EDTA solution were pipetted into the same centrifuge tube which contained the earlier pipetted out DMEM medium. After completing the trypsinization process, the centrifuge tube was centrifuged and cell viability was evaluated.

CHAPTER THREE

LASER-ASSISTED PRINTING OF GLYCEROL SOLUTION

3.1 Effects of Fluid Properties on Jet Formation

Time-resolved imaging analysis was performed in this study to obtain a better understanding of the material transfer process during MAPLE DW. Several events occur during a typical MAPLE DW process: bubble formation, jet formation/breakup and jet/droplet landing. During the direct-write process, the energy of the incident laser pulse is absorbed by the glycerol solution-based ribbon coating, producing a high pressure and high temperature bubble that forms and further expands within the coating due to sublimation [Lin2009b] [Wang2009]. Well-defined jets only form under certain operating conditions for a given glycerol solution. In particular, the jet formation process can be classified into four different scenarios depending on the laser fluence and the glycerol concentration: splashing (Fig. 3.1), jetting with bulgy shape (Fig. 3.2(a) and (b)), well-defined jetting (Fig. 3.2(c) and (d)), and no material transferred (Fig. 3.2(e)) as the glycerol concentration varied from 15% to 99% under a laser fluence of 717 ± 45 mJ/cm^2. The background of these figures is composed of two different regions: the top portion corresponds to the ribbon and its coating and the lower part the free space or ambient environment. There were some reflections of jetting phenomena on the ribbon, which

acted as a mirror during imaging. The phenomena observed herein when the concentration changed are consistent with others reported or discussed when operating conditions varied [Lin2009b] [Young2002] [Duocastella2009] [Guillemot2010a] during laser direct writing.

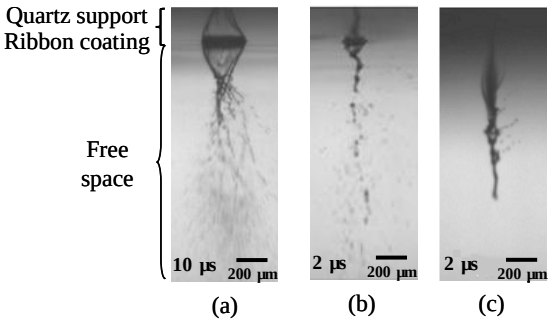

Fig. 3.1 Splashing regime using low glycerol concentration solutions: (a) 15%, (b) 25% and (c) 35%, and all under laser fluence of 717 ± 45 mJ/cm^2

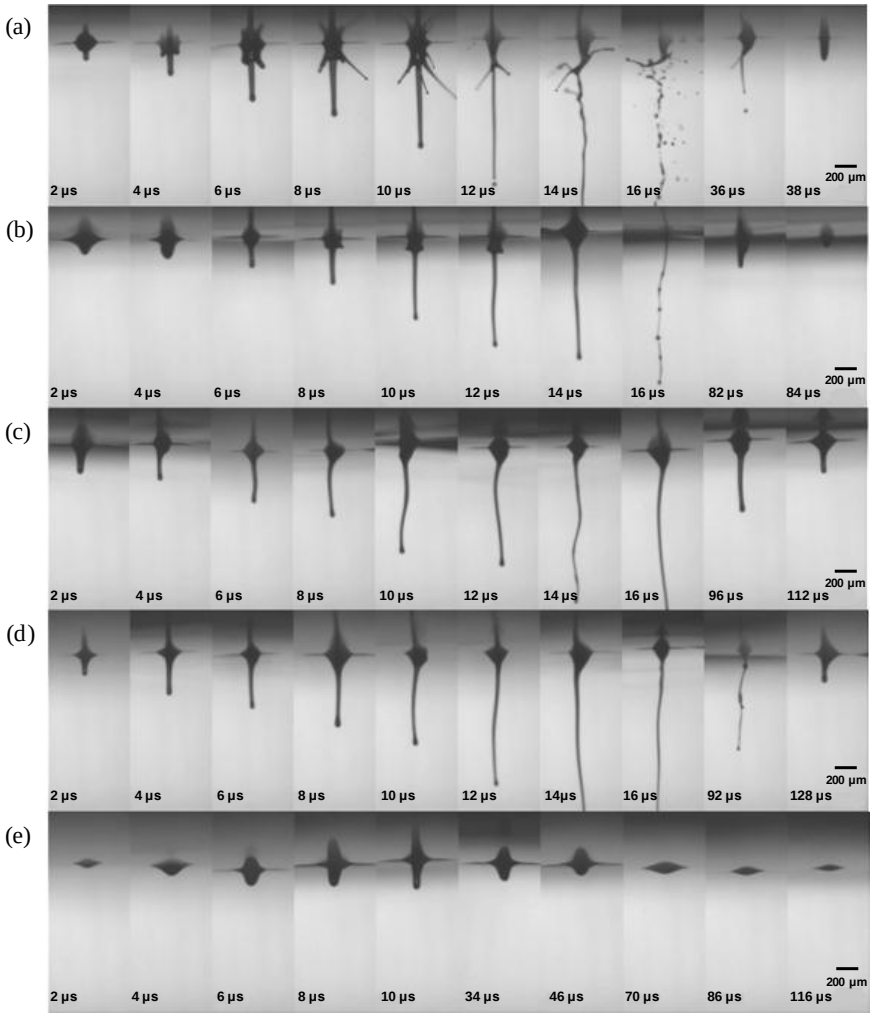

Fig.3.2 Different time-resolved representations of some jetting regimes (laser fluence = 717 ± 45 mJ/cm^2): (a) jetting with bulgy shape when using 50% solution, (b) jetting with bulgy shape when using 65% solution, (c) well-defined jetting when using 75% solution, (d) well-defined jetting when using 85% solution, and (e) no material transferred when using 99% solution

3.2 Typical Jetting Regimes

As aforementioned, four different jetting regimes have been observed in direct writing of glycerol solutions. Under the laser fluence of 717 ± 45 mJ/cm^2, splashing happened with the 15%, 25%, and 35% glycerol-water solutions as shown in Fig. 3.1. Fig. 3.3 further illustrates a time-resolved study of jet formation of 15% glycerol solution under laser fluence of 1433 ± 77 mJ/cm^2. The following discussion regarding the jetting regimes is based on the 717 ± 45 mJ/cm^2 laser fluence condition.

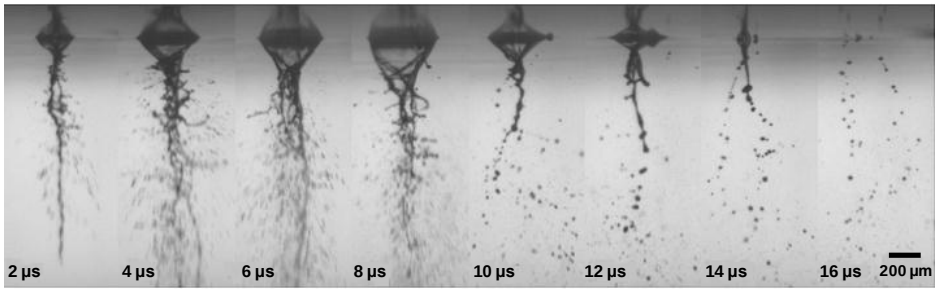

Fig. 3.3 Time-resolved images of jet formation of 15% glycerol solution under laser fluence of 1433 ± 77 mJ/cm^2

It can be seen that well-defined jets were difficult to form using the less viscous 15%, 25%, and 35% solutions under these investigated conditions. For the 15% and 25% solutions, splashing dominated the process, and burst of bubbles were visible at the ribbon coating. Since the 35% solution has a higher viscosity and a higher viscous damping force, it had a mixed appearance: splashing with bulgy shapes.

When the concentration was 50% or 65%, a jet formed but with a bulgy shape (Fig. 3.2(c) and (d)). Upon the expansion of laser-induced bubble, a protrusion first generated and elongated to form a long jet. Then bulge(s) formed around the forming main jet and further elongated out as little sub-jets. Finally, the main jet broke up with some residual protrusion materials remained and retracted to be part of the ribbon coating. The bulge appeared later when the concentration increased. The bulgy shape was most pronounced using the 50% glycerol solution, but not so observable with glycerol solutions having concentration lower than 50% or higher than 65%.

Well-defined jets were formed using the 75% and 85% solutions as shown in Fig. 3.2(c) and (d). Such a jet lasted longer when the concentration was higher. There was no material transferred using the 99% solution, and part of the ribbon coating protruded out but finally recoiled back without any fluid jetting. The recoiling process was slower for such a highly viscous solution, and the entire process lasted more than 100 μs.

As seen from Fig. 3.2, the temporally averaged jet velocity decreased as 122.2, 118.1, 93.4, 83.0, and 77.4 m/s when the glycerol concentration increased as 50%, 65%, 75%, 85%, and 99%, correspondingly. Intuitively, the jet formation process mainly is the result of two competing effects: the inertia effect to form and elongate the jet and the viscous damping effect to slow down the forming jet and dissipate the jetting energy. As such, the higher the viscosity, the lower the jet velocity.

3.3 Jetting Regime as Functions of Fluid Properties and Laser Fluence

Jetting during MAPLE DW is the result of the formation of laser-induced vapor/plasma bubble inside the ribbon coating. As the absorbed laser energy raises the solution temperature in the laser focal volume above the boiling temperature, the heated fluidic coating material undergoes a metastable superheated state [Lin2008]. Any slight perturbation in coating density may lead to the initiation of vapor nuclei in the superheated liquid, known as homogeneous nucleation; once vapor bubbles reach a critical size, their further growth is spontaneous and the superheated volume may explode [Yoo2001], leading to phase explosion, a form of rapid evaporation. When the internal bubble pressure reaches a balance with that due to the ambient pressure and the surface tension, the bubble has its largest size. As the bubble continues to grow, the internal bubble pressure becomes lower than that due to the ambient environment and surface tension. Then it shrinks and eventually collapses.

In this study, it is considered that the laser pulse-induced phase explosion contributes most to the generation of sublimation pressure, which ruptures the coating material beneath to form a jet or jets. It should be pointed out that laser pulse-induced thermoelastic stress [Wang2011] might also contribute to the jet formation in addition to phase explosion. The aforementioned scenario is also applicable to the sacrificial layer-assisted LIFT process, during which the bubble is induced by the expansion of a

vapor or plasma resulting from the ablation of sacrificial film [Schaffer2002] [Brujan2006].

The effect of glycerol concentration is summarized in Fig. 3.4 and some images are chosen to illustrate the different regimes under a laser fluence of 717 ± 45 mJ/cm^2. For the highest concentration solution (99%), the bubble pressure is not high enough to overcome the effect due to the ambient pressure and the surface tension, so no material is transferred. For the 85% and 75% solutions, a well-defined jet forms. The expanding bubble collapses outwards the coating instead of shrinking or collapsing inwards the coating. For the 65% and 50% solutions, a jet may form but with bulge(s) around it. As the laser-induced bubble expands, a high-pressure area forms between the bubble and the free surface. The formation of bulges is attributed to the collision of the liquid flows around the ablation spot [Unger2011] and/or the breakup of the main bubble when vapor bubble collapses inwards and/or bursts outwards the coating. This phenomenon is analogous to the evolution of cavitation bubble during ablation in liquid [Lauterborn1997] [Brujan2005]. For the 35%, 25% and 15% solutions, splashing and bubble bursting clearly reveal the effect of highly pressurized bubble, which bursts outwards the coating and even may atomize the coating being transferred.

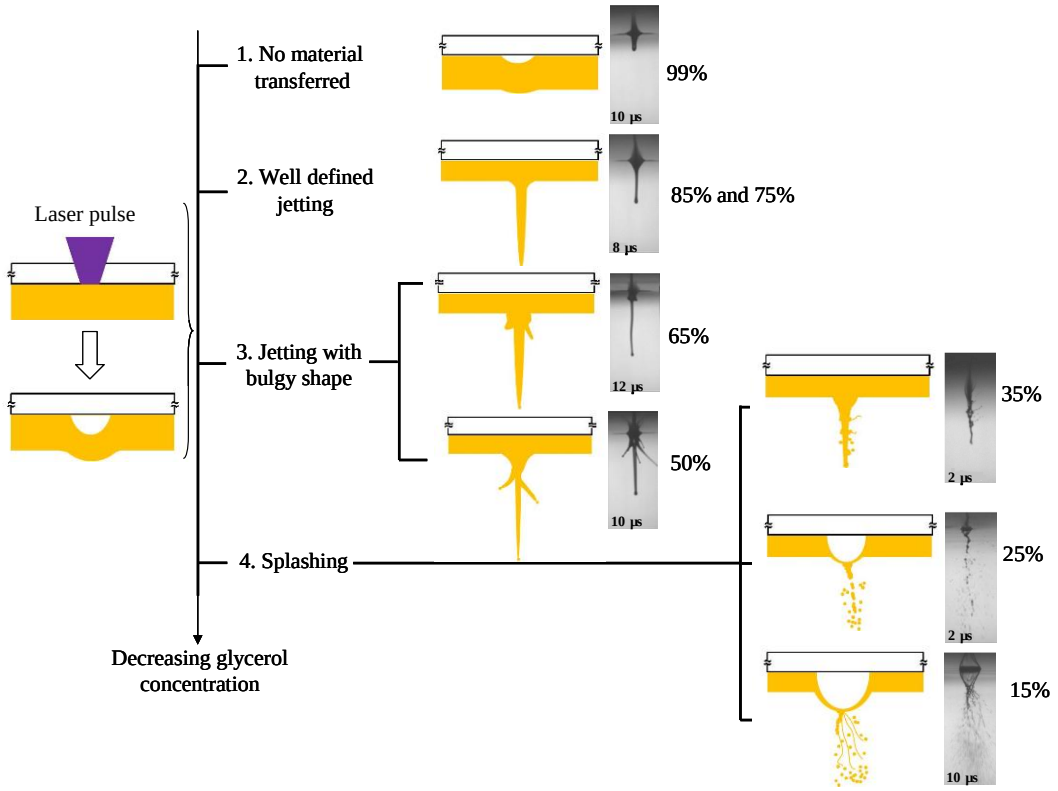

Fig. 3.4 Jetting regimes during MAPLE DW with different glycerol concentrations (laser fluence = 717 ±45 mJ/cm^2)

The effect of laser fluence on the jet formation has also been studied herein, and similar phenomena have been observed as previously reported [Young2002] [Duocastella2009] [Unger2011] [Brown2011]. Fig. 3.5 shows some representative jetting regimes during MAPLE DW using a 65% glycerol solution. Four jet formation regimes were also observed: no material transferred, well-defined jetting, jetting with bulgy shape, and splashing as the applied laser fluence increased. The laser fluence determines the jet kinetic energy, and higher laser fluences result in a higher jet/droplet velocity

[Young2002] [Duocastella2009] [Kaur2009]. The glycerol concentration affects the viscous dissipation energy and the capillary force. When the jet kinetic energy is higher than that due to viscous dissipation, a jet forms; when the surface tension effect dominates and leads to the Rayleigh instability, the jet breaks up, forming flying droplet(s).

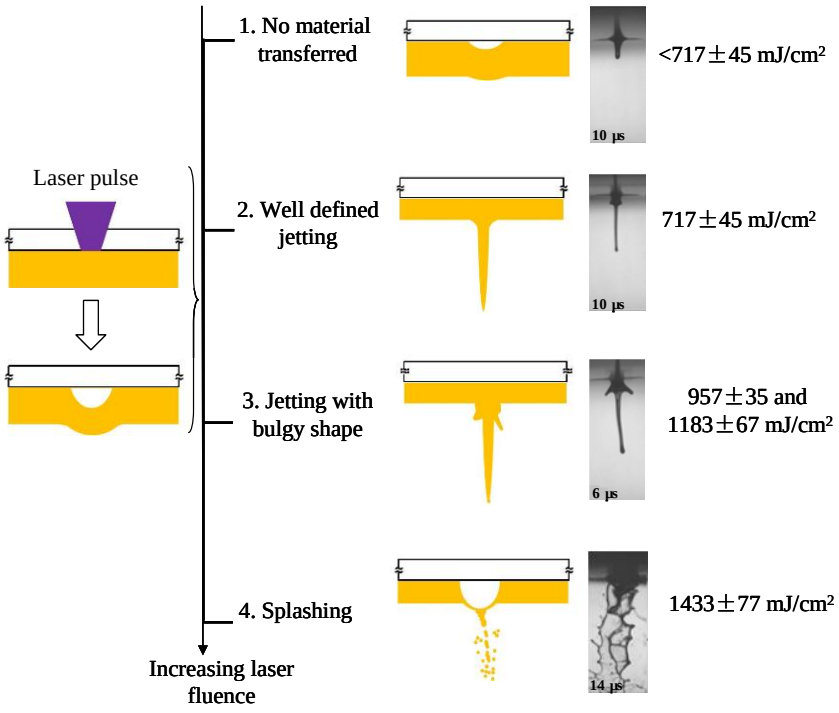

Fig. 3.5 Jetting regimes during MAPLE DW under different laser fluences (65% glycerol solution)

Under laser fluences lower than of 717 ±45 mJ/cm^2 such as 478 ±45 mJ/cm^2, no

material was transferred, and the bubble pressure did not exceed the pressure due to the surface tension of ribbon coating and the ambient environment. This is a similar scenario as shown in Fig. 3.2(e). Under a laser fluence of 717 ± 45 mJ/cm^2, well-defined jet formed as shown in Fig. 3.2(c) and (d). Under laser fluences of 957 ± 35 and 1183 ± 67 mJ/cm^2, the forming jet turned bulgy and curved as seen from Fig. 3.2(a) and (b). The higher the laser fluence, the more the coating material being transferred, resulting in a larger, but less stable jet. When the applied laser fluence was even higher such as 1433 ± 77 mJ/cm^2, splashing occurred instead of a jet, similar to those shown in Fig. 3.1. It should be noted that the laser fluence level for different jetting regimes varies as the coating solution changes.

In summary, jetting dynamics is a function of fluid properties such as the glycerol concentration and operating conditions such as the laser fluence. If the laser fluence is too low and/or the glycerol concentration is too high, it is less likely for a bubble to fully form and/or grow before it diminishes [Lin2008]. There is no enough kinetic energy provided by the expanding bubble. Even when a jet can be formed, it retracts back after the bubble diminishes. If the laser fluence is too high and/or the glycerol concentration is too low, it is also difficult to form a well-developed jet since dramatic bubble expansion may lead to a bulgy shape [Barron2005] and even splashing [Lin2009b] [Lin2008] [Unger2011]. Only under some selected conditions of glycerol concentration and laser

fluence as aforementioned, can a well-defined jet form.

3.4 Jettability in Laser Printing of Glycerol Solution

The droplet formation process on the printing quality has been of great research interest during drop-wise manufacturing, especially in terms of the printability [Jang2009] and the droplet formability [Herran2012a] [Herran2012b] during orifice-based inkjetting. Of different non-dimensional numbers used to quantify the process dynamics during the jet and/or droplet formation process, the Ohnesorge number (*Oh*) provides a convenient way of capturing the relative magnitudes of inertial, viscous, and capillary effects for such free-surface fluid mechanics problems [McKinley2011]. Generally, the Ohnesorge number can be determined as follows

$$Oh = \frac{\mu}{\sqrt{\rho \sigma l}} \tag{1}$$

where μ, ρ, and σ are the fluid viscosity, density, and surface tension, and l is the characteristic length which is taken as the laser spot diameter (150 μm in this study). As seen from Eq. (1), the Ohnesorge number only depends on the thermophysical properties (viscosity, density, and surface tension) of fluid and the laser spot size.

As discussed, a good jet only forms under certain combinations of fluid properties and operating conditions. For given operating conditions such as the laser fluence in this

study, a new non-dimensional *J* number, defined as the inverse of the Ohnesorge number, is proposed to evaluate the jettability during laser printing:

$$J = \frac{1}{Oh} \tag{2}$$

It is noted that the inverse of the Ohnesorge number has also been proposed as a non-dimensional *Z* number to quantify the fluid printability during inkjetting under a certain excitation voltage, and the printability was evaluated based on the single droplet formability, minimum stand-off distance, positional accuracy, and maximum allowable jetting frequency [Jang2009]. Alternatively, *J* can be also interpreted as the ratio between the viscous diffusion time scale t_μ and the Rayleigh time scale t_σ, which are defined, respectively, as follows:

$$J = \frac{t_\mu}{t_\sigma} \tag{3}$$

where $t_\mu = \frac{\rho l^2}{\mu}$ and $t_\sigma = \sqrt{\frac{\rho l^3}{\sigma}}$. Fig. 3.6 illustrates the relationships among *J*, the viscous diffusion and Rayleigh (capillary) time scales, and the glycerol concentration under a laser fluence of 717 ± 45 mJ/cm^2. As the glycerol concentration increases, the viscosity increases significantly while there are negligible variations with the density and surface tension [Lin2009], resulting in a deceasing *J*. Due to the same reason, the viscous diffusion time scale increases significantly while the Rayleigh time scale almost stays the same as the glycerol concentration decreases. As seen from Fig. 3.6, no materials are

transferred if the Rayleigh time is longer than the viscous diffusion time scale. Once the viscous diffusion time scale is longer than the Rayleigh time scale with a 85% glycerol solution, good jet forms; if the glycerol concentration further decreases, splashing may happen. The *J* values for 15%, 25%, 35%, 50%, 65%, 75%, 85%, and 99% solutions are 70.46, 48.54, 32.07, 14.61, 5.87, 2.49, 0.86, and 0.13, respectively, and the J value decreases almost exponentially with the glycerol concentration. It is observed that a good jet forms at $0.86 \leq J \leq 2.49$ (corresponding from 75% to 85%) in this study under the laser fluence of 717 ± 45 mJ/cm^2.

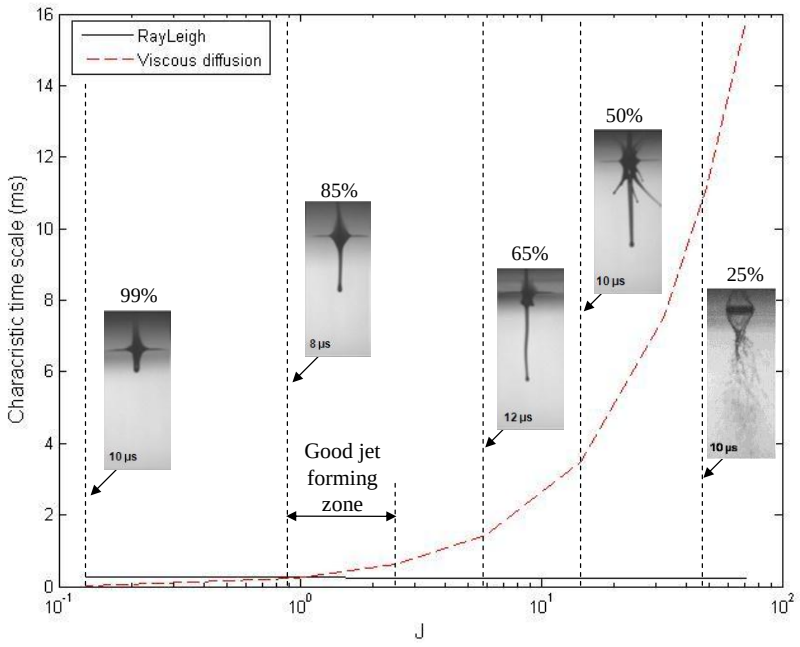

Fig. 3.6 Jetting regimes and characteristic time scale variations under laser fluence of 717 ± 45 mJ/cm^2

It should be noted that the jettability range varies as the laser fluence changes, which means the change of external forcing dynamics such as the jet velocity. Fig. 3.7 illustrates different jetting regimes (no materials transferred, good jet forming, and splashing/bulgy) delineated using dashed lines based on the experimental observations in this study as the laser fluence varies. Fig. 3.7(a) is based on the jettability number, *J*, while Fig. 3.7(a) is based on the glycerol concentration. The dashed lines are for illustration only, and more experiments are needed in future studies to exactly determine the line positions. To better appreciate the jettability, a non-dimensional numbers-based phase diagram, such as a diagram based on the Ohnesorge and Reynolds numbers for typical viscous fluids [McKinley2011], is expected by including the contributions from both the material properties and operating conditions.

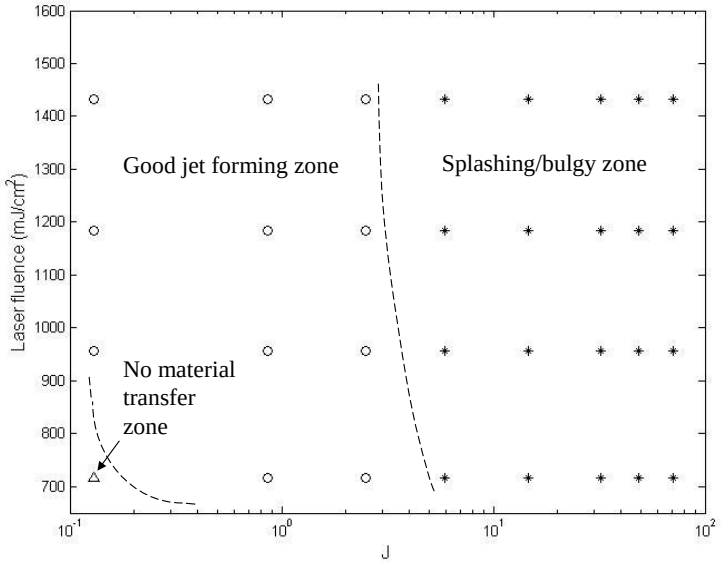

(a)

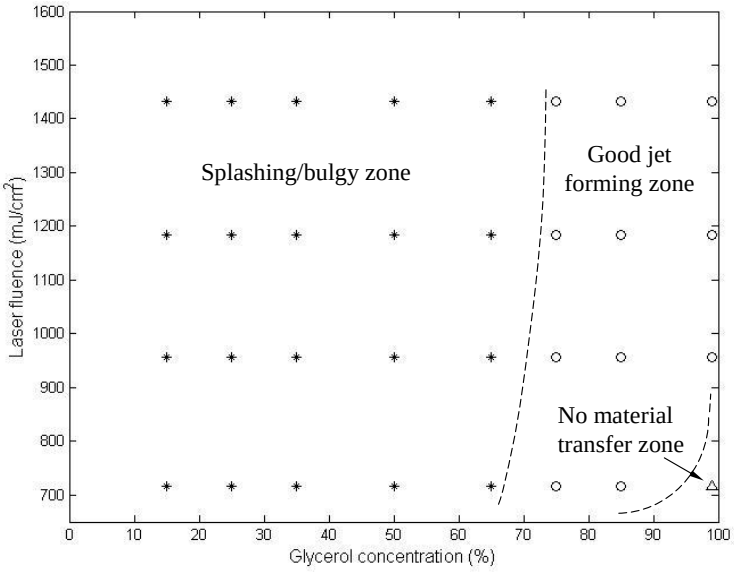

(b)

Fig. 3.7 The influence of glycerol concentration and laser fluence on jet morphology and printability (Dashed lines are for illustration only)

3.5 Conclusions

In this section, laser-assisted printing of glycerol solutions is studied. This section has investigated the effects of fluid properties as well as the combined effects of laser fluence and fluid properties on the jet formation process during laser-assisted printing of glycerol solutions. A time resolved imaging analysis-based approach has been implemented to investigate the jet formation process. It is found that the jetting dynamics is a function of fluid properties such as the glycerol concentration and operating conditions such as the laser fluence. If the laser fluence is too low and/or the glycerol concentration is too high, it is less likely for a bubble to fully form and/or grow before it diminishes. There is no enough kinetic energy provided by the expanding bubble. Even when a jet can be formed, it retracts back after the bubble diminishes. If the laser fluence is too high and/or the glycerol concentration is too low, it is also difficult to form a well-developed jet since dramatic bubble expansion may lead to a bulgy shape and even splashing. Only under some selected conditions of glycerol concentration and laser fluence, can a well-defined jet form. When a jetting fluid is given, its jettability (J) can be characterized as the inverse of Ohnesorge number. It is observed that a good jet forms at $0.86 \leq J \leq 2.49$ in this study under the laser fluence of 717 ± 45 mJ/cm^2.

CHAPTER FOUR

LASER-ASSISTED PRINTING OF SODIUM ALGINATE SOLUTION

4.1 Effect of Material Properties on Printing Process

Basically, there are several events occur during a typical MAPLE DW process: bubble formation, jet formation/breakup and jet/droplet landing. During laser-assisted printing, the energy of the incident laser pulse is absorbed by the alginate/glycerol solution-based ribbon coating, forming a high pressure and high temperature bubble that further expands within the coating due to sublimation [Barron2005] [Young2002].

The effect of material properties on the printing process is studied using 2%, 4% and 6% NaAlg solutions as printing ink. The laser fluence was initially controlled at 1021 $\pm$ 22 mJ/cm^2, the spot size was 150 μs, and the direct writing height was about 1.8 mm. The time-resolved typical images are shown in Fig. 4.1. The printing mechanism for 2% NaAlg is droplet contact-based instead of jet contact-based for 4% and 6%, and this droplet contact-based printing has not been reported thus far as of laser-assisted printing. It can be seen from Fig. 4.1(a), a droplet emerged under the tip of the main jet within the first 100 μs. Then more droplets formed upon contacting the receiving substrate. From 200 to 300 μs, more droplets were formed and “beads-on-a-string” (BOAS) phenomenon was observed, which was previous observed by Unger et al. [Unger2011], but without a

receiving substrate. Within this time duration, the initial laser-induced bubble shrank back and became smaller until could hardly be seen. The entire printing process lasted for about 300-400 μs. For 4% and 6% NaAlg, the main jet contacted the receiving substrate before droplet formation. The droplets formed by the thinning of the main jet, which was due to Rayleigh instability. As can be seen from Fig. 4.1, droplets started to emerge as BOAS at 100-200 μs and 200-300 μs for 4% and 6% NaAlg solutions respectively. There was no exact time to define the breakup of the jet since local BOAS still presented until posterior frames. The entire printing process lasted for about 500-600 μs and 600-700 μs for 4% and 6% solutions respectively.

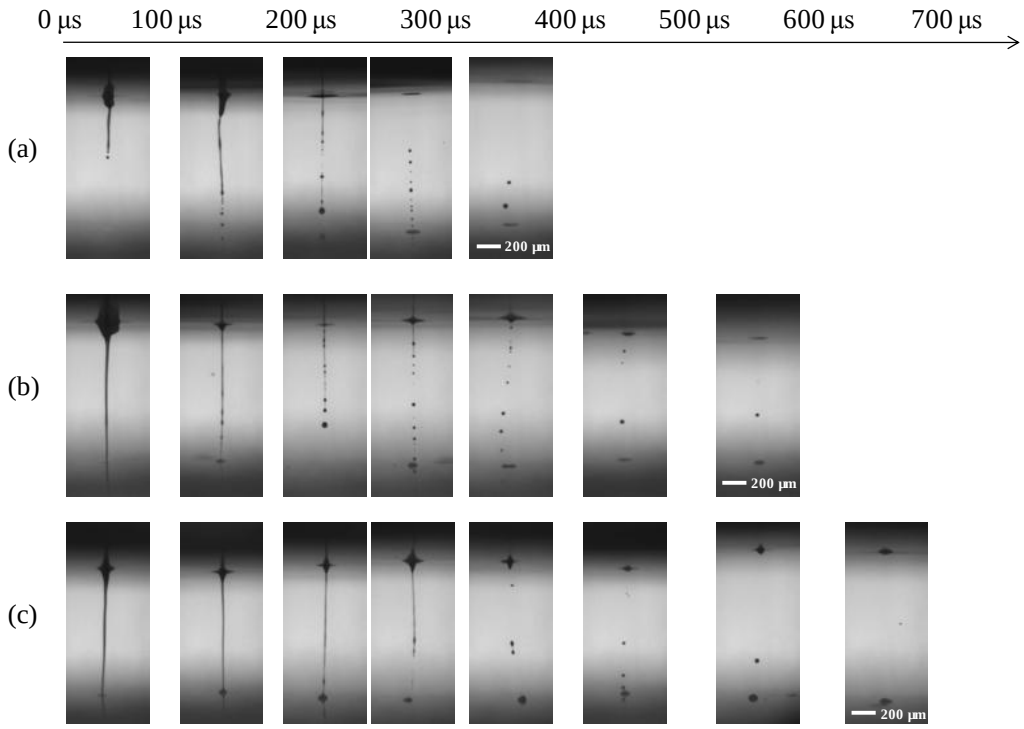

Fig. 4.1 Time-resolved representative images of alginate printing process (laser fluence 1021 ± 22 mJ/cm^2, laser spot size 150 μm, and direct writing height 1.8 mm): (a) 2% NaAlg, (b) 4% NaAlg, and (c) 6% NaAlg

The physical properties of viscoelastic fluid NaAlg vary among different concentrations. The density increases while surface tension decreases with the increase of NaAlg concentration, as can be seen from Table 1. However, the amplitudes of variation are small (about 4%). The viscosity increased at a large extent (about 23 times) as the NaAlg concentration increases from 2% to 6%. Therefore, higher concentration fluid is much more viscous. The Ohnesorge number is a nondimensional number that

characterizes the balance of viscous, surface tension and inertial effects of a slender filament. Generally, the Ohnesorge number can be determined as follows:

$$Oh = \frac{\mu}{\sqrt{\rho \sigma l}} \tag{4}$$

where μ, ρ, and σ are the fluid viscosity, density, and surface tension, and *l* is the characteristic length which is taken as the laser spot diameter. Alternatively, Ohnesorge number can be also interpreted as the ratio of the Rayleigh time scale t_σ and the viscous diffusion time scale t_μ, which are defined respectively as follows:

$$Oh = \frac{t_\sigma}{t_\mu} \tag{5}$$

where $t_\sigma = \sqrt{\frac{\rho l^3}{\sigma}}$, and $t_\mu = \frac{\rho l^2}{\mu}$. The Ohnesorge number is dependent only on material properties and characteristic length. The calculated Ohnesorge numbers are 1.59, 10.64 and 37.47 for 2%, 4% and 6% NaAlg solutions respectively. A larger Ohnesorge number indicates the domination of viscous force. According to experimental results, a larger Ohnesorge number indicates a larger tendency of jet contact-based printing, while a smaller Ohnesorge number indicates a larger tendency of droplet contact-based printing.

In order to understand the effect of viscoelasticity on jet formation, the fluid must be characterized. Relaxation time is the unique property of viscoelastic fluid, and it is preferentially examined herein. The longest relaxation time, which is the time for the molecular chins to return to rest after they are released from a stretched position, has

typically been determined using Zimm model [Yan2011] [Cooper-White2002]. The Zimm model defines the relaxation time as:

$$\lambda_Z \cong \frac{1}{\zeta(3\upsilon)} \frac{[\eta] M_W \eta_s}{N_A k_B T} \tag{6}$$

$$[\eta] = A(M_W)^{\alpha} \tag{7}$$

where $[\eta]$ is the intrinsic viscosity, M_W is the molecular weight and is calculated as 24 kDa (24000 g/mol), η_s is the solvent viscosity (deionized water ~1 mPa s), N_A is Avogadro's constant, k_B is the Boltzmann constant, and T is the temperature in Kelvin (298K).

The empirical constants for $[\eta]$ is found to be A=0.00504 and α=1.01 [Vold2006]. It was calculated that $[\eta] = 133.8\, ml \cdot g^{-1}$, the Zimm constant $\frac{1}{\zeta(3\upsilon)} = 0.60235$, and $\lambda_Z = 0.78\, ms$. The inverse of the intrinsic viscosity is the critical overlap concentration $c^* = \frac{0.77}{[\eta]} = 0.0058\, g/ml$, which is defined by Graessley [Graessley1980]. The effective relaxation times for 1% and 2% NaAlg solutions have been calculated as 1.1 ms and 2.15 ms respectively according to experiment data. The calculated values are listed in Table 2. Effective relaxation times for 4% and 6% NaAlg solutions are estimated based on the linear relationship of linear relationship between $\lambda_{eff} / \lambda_Z$ and c / c^* [Tirtaatmadja2006] in this study, as can be seen from Fig. 4.2. The prediction values of λ_{eff} is also shown in Table 2.

Table 2 Calculation of effective relaxation time of NaAlg

c (g/ml)	c^* (g/ml)	λ_{eff} (ms)	λ_Z (ms)	c/c^*	λ_{eff}/λ_Z
1%	0.0058	1.10	0.78	1.72	1.41
2%		2.15		3.45	2.76
4%		4.17		6.90	5.34
6%		6.33		10.34	8.12

The Deborah number De balances the viscous and the elastic effects, which is interpreted as the ratio of the relaxation time scale λ_{eff} and the Rayleigh time scale t_σ:

$$De = \frac{\lambda_{eff}}{t_\sigma} \tag{8}$$

It can also be represented as:

$$De = \sqrt{\frac{{\lambda_{eff}}^2 \sigma}{\rho l^3}} \tag{9}$$

The Deborah number is also dependent only on material properties and characteristic length. The calculated Deborah numbers are 7.96, 14.89 and 21.83 respectively for 2%, 4% and 6% NaAlg solutions. The smaller the Deborah number, the ink behaves more fluid like. A larger Deborah number indicates the increasing domination of elasticity,

reaching solid like behavior. According to the experimental results, regardless of laser fluence, 4% and 6% NaAlg solutions were more difficult to print than 2% solution (as can be seen under the laser fluence of 800 mJ/cm^2). In addition, it was more likely to have jet contact-based printing than droplet contact-based printing with larger Deborah number, indicating the elastic behavior of the ink that "stretched" the fluid into a long thin jet.

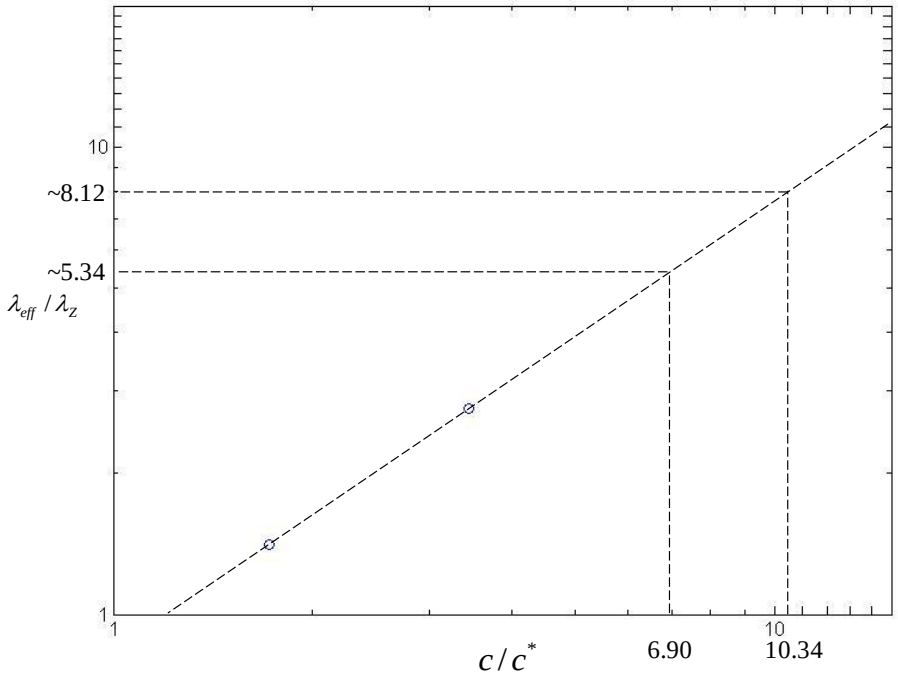

Fig. 4.2 Prediction of λ_{eff} of 4% and 6% NaAlg solutions based on linear relationship between λ_{eff}/λ_Z and c/c^*

4.2 Effect of Laser Fluence on Printing Process

The effects of different operating conditions on the printing process are investigated in this study in order to better understand the printing mechanism. The operating conditions can affect the entire printing process, from bubble formation, jet formation, jet development, droplet formation to the final landing process. Basically, the operating conditions include laser fluence, laser spot size and direct writing height, and they are supposed to have similar or counterpart effects as material properties.

Various laser fluences were used to print different concentrations of NaAlg solutions in order to investigate the effect of laser fluence on the printing process. As stated above, the printing phenomenon can be generally divided into several different regimes: splashing, jetting and no deposition. Since only a single deposition spot is preferred during printing, it is defined as "printable" in this study only when a well defined jet or droplets in a straight line can be obtained. Basically, the laser fluences used in this study are in the "printable" regime.

Fig. 4.3 shows the representative images of the printing of 2% NaAlg solution using laser fluences of 686 ± 19, 861 ± 20, 1021 ± 22, 1196 ± 29, and 1380 ± 34 mJ/cm^2 respectively. One representative image is shown for every 100 μs for each case. When the ink is locally superheated, the pulse energy is converted to the bubble expansion energy which ejects the ink away and forms a jet. Once the jet forms, surface tension will try to

thin and pinch off the jet, and then the jet breaks up into droplet(s) due to Rayleigh instability. At the same time, the jet develops towards the receiving substrate with a velocity of tens of meters per second impelled by bubble expansion. The thinning velocity or capillary velocity of the jet is defined as the decreasing rate of the radius of the jet R: $U = -\frac{dR}{dt}$. Theoretically, if the jet arrives at the receiving substrate faster than the breakup, droplets cannot be observed, resulting in jet contact-based printing. In contrast, if breakup velocity is fast, droplet contact-based printing can be observed.

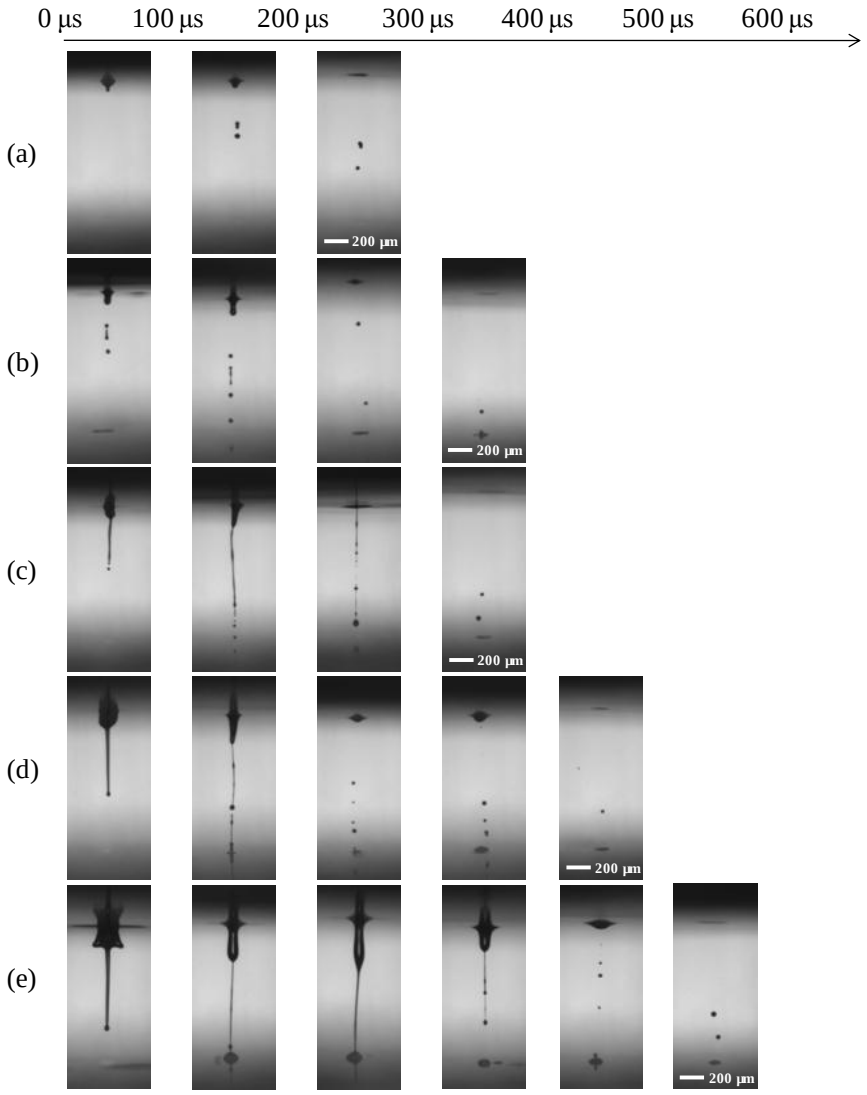

Fig. 4.3 Time-resolved representative images of alginate printing process (NaAlg concentration 2%, laser spot size 150 μm, and direct writing height 1.8 mm) at laser fluences of: (a) 686 ± 19 mJ/cm^2, (b) 861 ± 20 mJ/cm^2, (c) 1021 ± 22 mJ/cm^2, (d) 1196 ± 29 mJ/cm^2, and (e) 1380 ± 34 mJ/cm^2

In this study, droplet contact-based printing was obtained at laser fluences of 686 $\pm$ 19, 861 $\pm$ 20, 1021 $\pm$ 22 mJ/cm^2 (Fig. 4.3(a), (b) and (c)), while jet contact-based printing was obtained at 1196 $\pm$ 29, and 1380 $\pm$ 34 mJ/cm^2 laser fluences (Fig. 4.3(d) and (e)). Laser fluence can also influence the jetting dynamics besides fluid properties. At higher laser fluences, more energy was converted to bubble expansion energy, obtaining a jet with larger velocity. Consequently, the jet reached the receiving substrate earlier than the breakup of the jet, ending up jet contact-based printing. At lower laser fluences, the jet velocity is not larger enough so that the breakup of the jet can be seen before the jet contacting with the receiving substrate. It can be seen from Fig. 4.3 that the entire printing time increased monotonically with the laser fluence. For example, at the laser fluence of 686 $\pm$ 19 mJ/cm^2, the initiated protrusion began to shrink much earlier and ends also much earlier than higher laser fluences. This is because when subjected to higher laser fluences, more ink is ejected away from the ribbon, and it takes more time to break and end up the jet, overcoming the contribution of a high speed jet induced by a higher laser fluence. In addition, the jet breakup appears earlier at lower laser fluences. This is also mainly due to the smaller jet velocity induced by low laser fluence, allowing the emerging of jet breakup before the jet contacting the receiving substrate. When subjected to higher laser fluences, the breakup of the jet appears after the jet contacts the receiving substrate, and the deposition point is then filled by the breaking droplets.

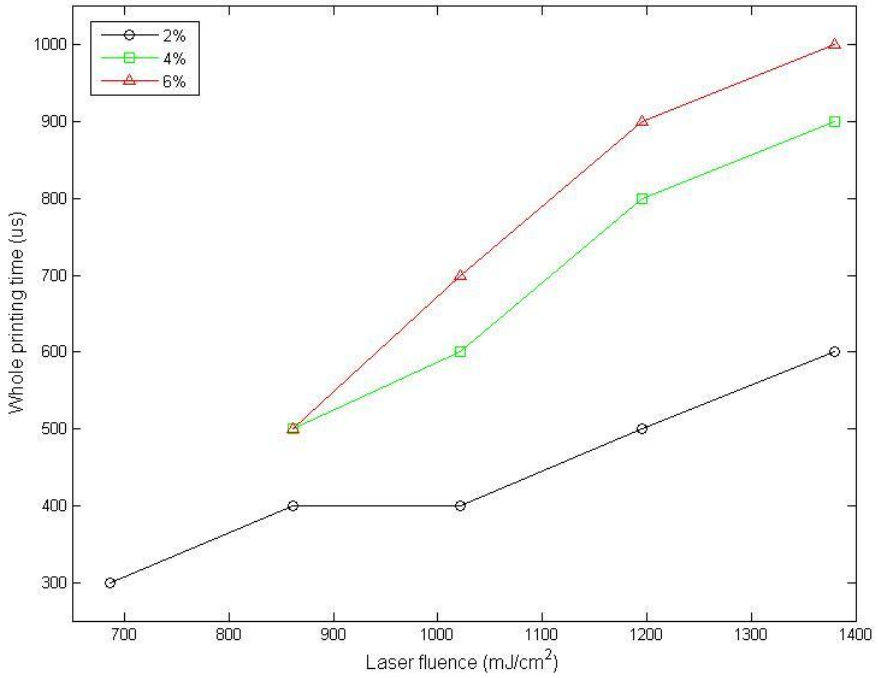

Fig. 4.4 The entire printing time as functions of laser fluence and NaAlg concentration

The results of printing 4% and 6% NaAlg solutions also show that the entire printing time increases with the laser fluence, as can be seen in Fig. 4.4. It can also be seen that the entire printing time increases with NaAlg concentration, which has been demonstrated in the previous section. What needs to be mention is that when 4% and 6% NaAlg solutions were used at the laser fluence of 686 $\pm$ 19 mJ/cm^2, no jet formed and thus no material was deposited, which means the laser fluence was too low to print the higher viscous material.

Moreover, the bubble formed at the laser fluence of 1380 $\pm$ 34 mJ/cm^2 was larger

than at lower laser fluences, and a bulgy shape was formed at the beginning, which has also been previously observed [Yan2012] [Unger2011]. Similar as Fig. 4.1, the BOAS phenomenon can also be seen in Fig. 4.3(c), (d) and (e). Since the development of the jet is not very stable even at the same printing condition, detailed morphology and breakup process is hence not emphasized here.

A variation of laser fluence indicates the variation of Reynolds number (*Re*). The Reynolds number is a dimensionless number that measures the ratio of inertial force to viscous force, and it is often used to characterize different flow regimes. The Reynolds number is defined as:

$$Re = \frac{\rho v l}{\mu} \tag{10}$$

Where ρ, μ, v, and l are the fluid density, viscosity, jet velocity, and characteristic length, which is taken as the laser spot diameter. The calculated Reynolds numbers are shown in Table 3. It can be seen that the Reynolds number increases with the laser fluence while decreases with NaAlg concentration. It can also be seen that Reynolds number increased with laser fluence more with lower concentration solution than higher concentration solution. The larger the Reynolds number, the larger the jet velocity, and thus the likely it would be to obtain jet contact-based printing.

Table 3 Calculation of Reynolds numbers under different printing conditions

Concentration\laser fluence (mJ/cm^2)	686 ± 19	861 ± 20	1021 ± 22	1196 ± 29	1380 ± 34
2%	1.33	13.46	15.19	18.41	32.85
4%	No jet	5.01	7.84	10.20	25.29
6%		1.12	1.62	2.13	3.49

4.3 Effect of Laser Spot Size on Printing Process

In order to study the effect of laser spot size in printing process, two different laser spot sizes were used in this study. The laser spot size used in the previous sections was 150 μm in diameter, while in this section a smaller laser spot size (50 μm in diameter) was used. Same laser fluences were used as comparison, as can be seen in Fig. 4.5. However, when 686 ± 19 mJ/cm^2 and 861 ± 20 mJ/cm^2 were used to print 2% NaAlg with a smaller spot size, no material was transferred. The 2% NaAlg solution was only printable under higher laser fluences (1021 ± 22 mJ/cm^2, 1196 ± 29 mJ/cm^2 and 1380 ± 34 mJ/cm^2) using laser spot size of 50 μm in diameter. Moreover, 4% and 6% NaAlg solutions were also not printable in the applied laser fluence range.

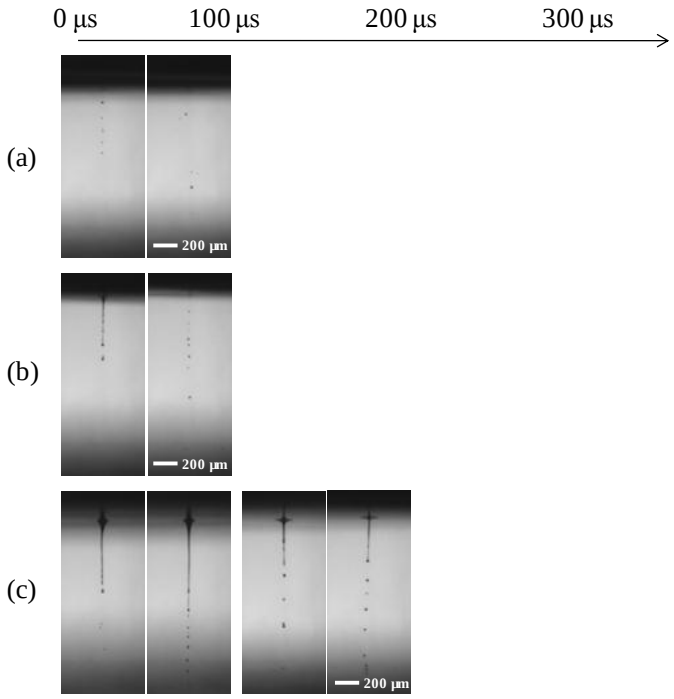

Fig. 4.5 Time-resolved representative images of alginate printing process (NaAlg concentration 2%, laser spot size 50 μm, and direct writing height 1.8 mm) at laser fluences of: (a) 1021 ± 22 mJ/cm^2, (b) 1196 ± 29 mJ/cm^2, and (c) 1380 ± 34 mJ/cm^2

Comparing the printing processes in Fig. 4.3 and Fig. 4.5, when smaller laser spot size was used, the jet became much thinner and droplets became much smaller. Hence the breakup of jet can be observed in the earlier time frames. It can also be seen that when a smaller laser spot size was used, the jet ended up much earlier, and the entire printing process lasted for less than 200 μs. By using a smaller laser spot size, less beam energy was transferred per pass. Therefore the initiated bubble was smaller, and the expansion energy was also less. Consequently, the jet velocity became smaller, resulting in droplet

contact-based printing. It can be seen in Table 4 that under laser fluence of 1021 ± 22 mJ/cm^2, the printing was droplet contact-based under both laser spot sizes. The printing changed from jet contact-based to droplet contact-based while using the laser fluences of 1196 ± 29 and 1380 ± 34 mJ/cm^2. BOAS phenomenon can be only observed under laser fluence of 1380 ± 34 mJ/cm^2. This is probably because if less material is transferred, jet is thinner, thus droplets are easier to form due to surface tension. Moreover, the thin filament is easier to be broke up as jet develops. Therefore, BOAS phenomenon only emerges when sufficient ink is ejected.

Table 4 Printing of 2% NaAlg under different laser spot sizes

Laser fluence (mJ/cm^2)\laser spot size (diameter/μm)	150	50
686 ± 19	Droplet contact-based	No material transferred
861 ± 20	Droplet contact-based	
1021 ± 22	Droplet contact-based	Droplet contact-based
1196 ± 29	Jet contact-based	Droplet contact-based
1380 ± 34	Jet contact-based	Droplet contact-based

Note: no material transferred for 4% and 6% NaAlg

4.4 Effect of Direct Writing Height on Printing Process

Another operating condition is direct writing height, which is the distance between the ribbon coating and the receiving substrate. Intuitively, breakup of jet is more likely to take place with a larger direct writing height. In this way, it is more likely to

have droplet contact-based printing using a larger direct writing height.

Experimental study was conducted to verify and further understand the effect of direct writing height in laser-assisted printing. Fig. 4.6 shows the time-resolved printing of 2% NaAlg solution at laser fluence of 1021 $\pm$ 22 mJ/cm^2, and the laser spot size used was 150 μm in diameter. The direct writing heights used were 1.8, 1.4, 1.0 and 0.5 mm. It can be seen that when the direct writing height was reduced from 1.8 mm to 1.4 mm, the printing remained droplet contact-based and the entire printing time did not change much (300-400 μs). However, the printing became jet contact-based when the direct writing height was reduced to 1.0 mm and smaller, and the entire printing time also changed to a bit longer (400-500 μs). The jet began to breakup within the first 100 μs at direct writing heights of 1.8 and 1.4 mm, while the jet began to breakup at 200-300 μs and 400-400 μs respectively at direct writing heights of 1.0 and 0.5 mm. The smaller direct writing height tended to "stable" the jet, as in Fig. 4.6(d), the jet was straight and thick within the first 400 μs. This stabilization effect was also found by Unger et al. [Unger 2011] that the appearance of a receiving substrate stabilized the jet. At a smaller direct writing height, the breakup of the jet was too quick that the jet ends up in the next 100 μs, and without any droplets floating in the air gap. Similarly, the jet travelled in a smaller distance when the direct writing height was smaller, and there is not sufficient time for the jet to breakup before it reached the receiving substrate. The BOAS phenomenon occurred at the direct

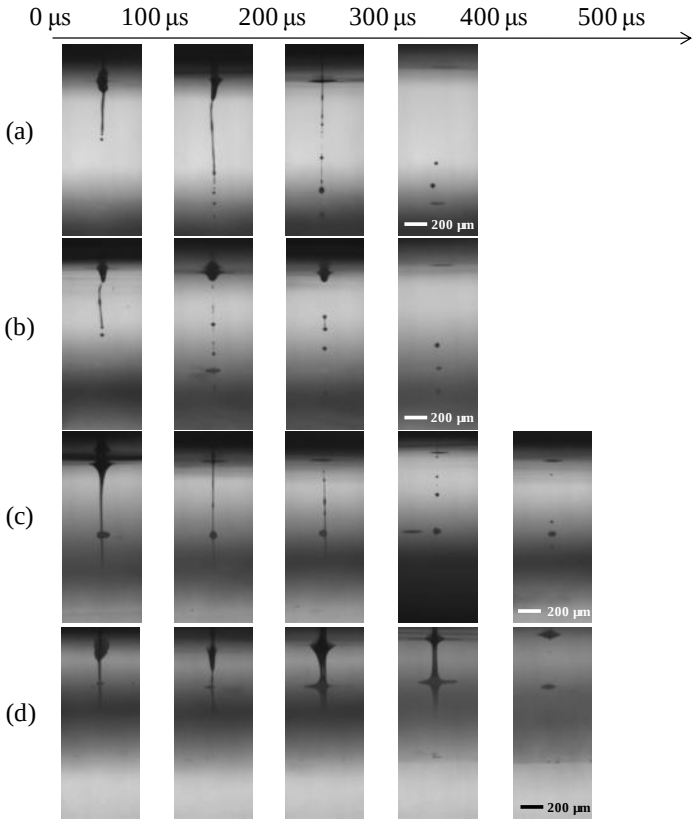

Fig. 4.6 Time-resolved representative images of alginate printing process (NaAlg concentration 2%, laser spot size 150 μm, and laser fluence 1021 ± 22 mJ/cm^2) at direct writing heights of: (a) 1.8 mm (b) 1.4 mm (c) 1.0 mm, and (d) 0.5 mm

writing heights of 1.8, 1.4 and 1.0 mm, but cannot be observed at direct writing height of 0.5 mm. Therefore, BOAS phenomenon only emerges when the jet travelling distance is sufficient. The results are similar when using other concentrations of NaAlg solutions.

4.5 Delineation of Printing Regimes

Generally, the printing type is divided into three different regimes according to

different fluid properties and operating conditions in this study. The schematic of the printing regime is shown in Fig. 4.7. The corresponding printing conditions for each regime have been discussed in the previous sections. During laser-assisted printing process, it is preferred to have jet contact-based printing rather than droplet contact-based printing considering the possible manufacturing application of this technique. On the one hand, the printing resolution could be higher for jet contact-based printing, especially a straight jet contact-based printing. On the other hand, micro droplets formed by jet breakup might be floating in the air gap and thus generating multi-deposition at one destination point at receiving substrate.

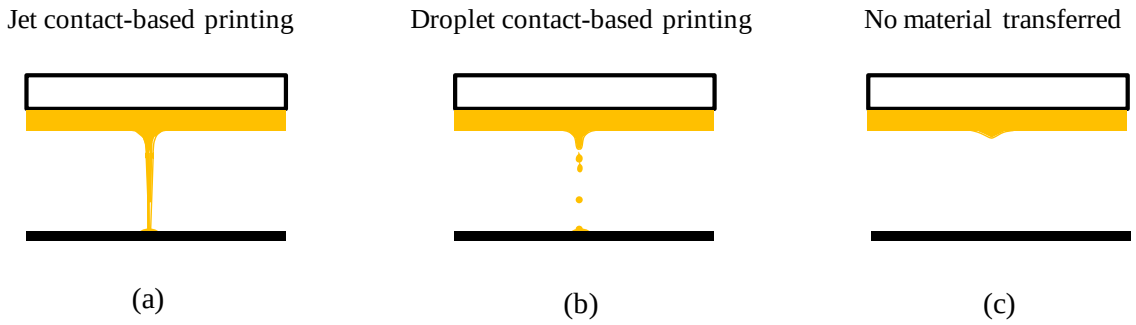

Fig. 4.7 Schematics of different printing regimes

An operating diagram is drawn by combining the fluid properties and operating conditions based on experimental results and physical understanding, as shown in Fig. 4.8. This logarithmic operating diagram is constructed under the laser spot size of 150 μm

and direct writing height of 1.8 mm, and it does not fully apply to other operating conditions. From this diagram, the preferable jet contact-based printing zone locates in the upper right part where both Deborah number and Reynolds number are sufficiently large. The droplet contact-based printing zone locates at the region that Deborah number is relatively small. When the Reynolds number is small and the Deborah number is relatively large, there is no material transferred. This is reasonable since a larger laser fluence indicates a larger Reynolds number, and a higher concentration solution indicates a larger Deborah number.

The Deborah number is only related to material properties and characteristic length, while the Reynolds number depends not only on material properties, but also on jet velocity and characteristic length. NaAlg concentration affects the material properties, laser fluence affects the jet velocity, and the laser spot size affects the characteristic length and jet velocity, while direct writing height affects none of the properties. Therefore, both dimensionless numbers would change with NaAlg concentration and laser spot size. However, Deborah number would probably not change with laser fluence. Moreover, both dimensionless numbers would not change with direct writing height. Therefore, more detailed understanding is expected in order to understand the printing regimes under different printing conditions.

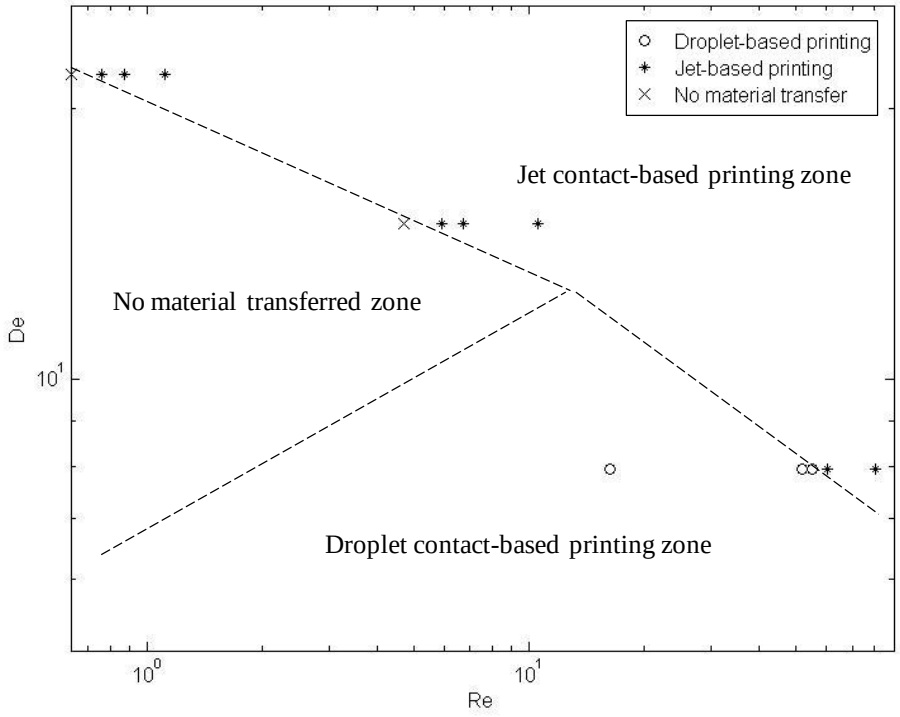

Fig. 4.8 Logarithmic operating diagram demonstrating different printing regimes (laser spot size 150 μm, direct writing height 1.8 mm)

4.6 Comparison of Viscoelastic and Newtonian Inks during Printing

The jet breakup for viscoelastic fluid and Newtonian fluid has been studied so far in the field of inkjet printing. However, the breakup time as well as the entire printing time in laser-assisted printing remains unclear. In this study, 85% glycerol solution was laser printed as a comparison with 2% NaAlg solution since they have the same zero-shear viscosity. The glycerol solution was used as a sample for Newtonian fluid,

while the NaAlg solution was used as a sample for viscoelastic fluid, which is also classified as non-Newtonian fluid.

Fig. 4.9 shows representative images at different time frames for printing of 85% glycerol and 2% NaAlg solutions at laser fluence of 1021 $\pm$ 22 mJ/cm^2. The laser spot size was kept at 150μm and the direct writing height was kept at 1.8 mm. The study of comparing the jet velocity of both Newtonian and viscoelastic fluids in laser-assisted printing is lacking, and it has been only known that the initial development velocity is faster for viscoelastic with high viscosity in inkjet printing [Clasen2011]. Fig. 4.9 shows that the jet velocity of viscoelastic fluid was much faster than that of Newtonian fluid. The jet broke up within the first 100 μs for 2% NaAlg solution, while it did not break up until 400-500 μs for 85% glycerol solution. The entire printing time for the viscoelastic fluid was about 300-400 μs, while it lasted for 700-800 μs for Newtonian fluid. Moreover, the breakup of the jet occurred also much earlier for the viscoelastic fluid.

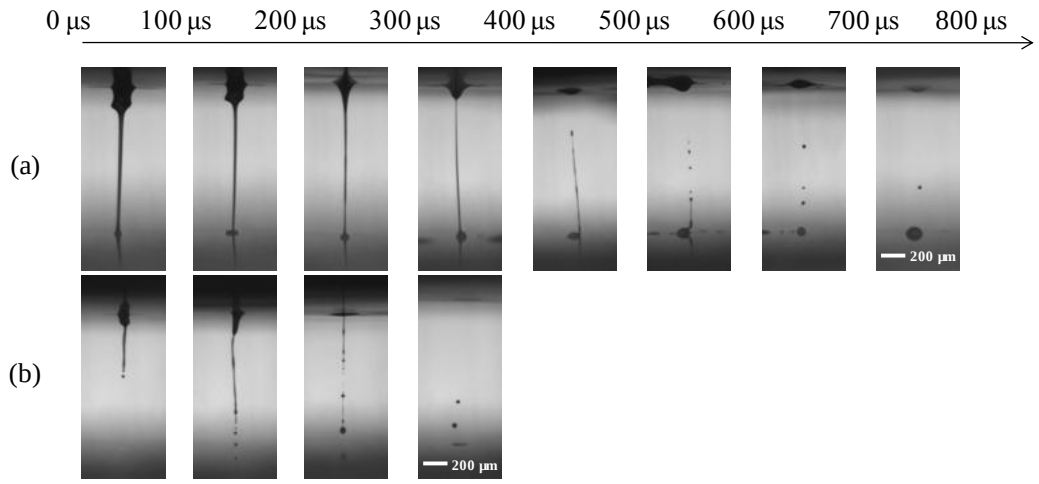

Fig. 4.9 Time-resolved representative images of laser-assisted printing process: (a) 85% glycerol, and (b) 2% NaAlg solution (laser spot size 150 μm, laser fluence 1021 ± 22 mJ/cm^2, and direct writing height 1.8 mm)

Though the result seems deviated from intuition, the more important mechanism for this result might be related with the difference of surface tension. The surface tension of 85% glycerol solution is 64.9 mN/m, which is much larger than that of 2% NaAlg solution (45.64 mN/m). Moreover, the density of 85% glycerol solution is 1.23 g/cm^3, which is also larger than that of 2% NaAlg solution (1.02 g/cm^3). Both surface tension effect and gravity force contribute to the ribbon coating thickness at the incidence of laser beam. The surface tension effect and gravity force serves as increasing the coating thickness in the middle part of ribbon. Therefore, as bubble expanded, more fluid can be ejected when printing the 85% glycerol solution. This can be proved from the earlier time

frames in Fig. 4.9(a) that the bubble was larger and the jet was thicker. As a result, the jet broke up much later and even the breakup process lasted for 400 μs. Despite the different laser fluences and different NaAlg concentrations used, the BOAS phenomenon is much more likely to emerge for viscoelastic fluid than Newtonian fluid. Even the breakup process lasted for as long as 400 μs for the Newtonian fluid, there was no BOAS phenomenon.

4.7 Conclusions

Laser-assisted printing of both viscoelastic and Newtonian fluids are investigated in this section in order to better understand the effects of printing parameters on printing process. Time-resolved imaging analysis is carried to study the effects of fluid properties and operating conditions including laser fluence, laser spot size and direct writing height in terms of the jet development process and jet morphology. It is found that the jetting dynamics is functions of both material properties and operating conditions. Both Ohnesorge number and Deborah number increase while Reynolds number decreases with NaAlg concentration. As of laser fluence, only Reynolds number is influenced and it increases with the laser fluence. It is also found that the entire printing time increases with both NaAlg concentration and laser fluence. In addition, the entire printing time decreases with laser spot size and direct writing height. Comparing the printing of

glycerol and NaAlg solutions with the same zero-shear viscosity, the entire printing time is much larger for the glycerol solution, and the jet breaks up later. An operating diagram relating Deborah number and Reynolds number is constructed for dividing the different printing regimes: jet contact-based printing, droplet contact-based printing and no deposition. In order to obtain the jet contact-based printing, relatively larger Deborah number and Reynolds number are needed. BOAS phenomenon has been observed in different cases in this study. It is demonstrated that BOAS phenomena can be only observed under higher laser fluences and higher concentration NaAlg solutions.

CHAPTER FIVE

LASER-ASSISTED PRINTING OF TUBULAR STRUCTURES

5.1 Laser-Assisted Printing of Alginate Tubes and Annular Constructs

5.1.1 Representative Alginate Tubes

Fig. 5.1(a) shows a representative alginate long tube printed using the proposed laser printing technique, and the height of the tube is about 6 mm. This tube was printed using an 8% NaAlg solution under a laser fluence of 1698 $\pm$ 45 mJ/cm^2. The tube was made with 240 layers and it has an average wall thickness of 0.8 mm and an outer diameter of 3.3 mm. For further illustration, Fig. 5.1(b) and (c) shows the top and side views of two different tubes. Generally, the wall surface is rough and the tube top layer is not flat, which might be due to the pulse instability of the excimer laser and/or the spreading of deposited droplets during landing. While some promising results have been achieved in terms of the overall feasibility, some process optimization work is expected in future studies in order to improve the overall printing stability and quality.

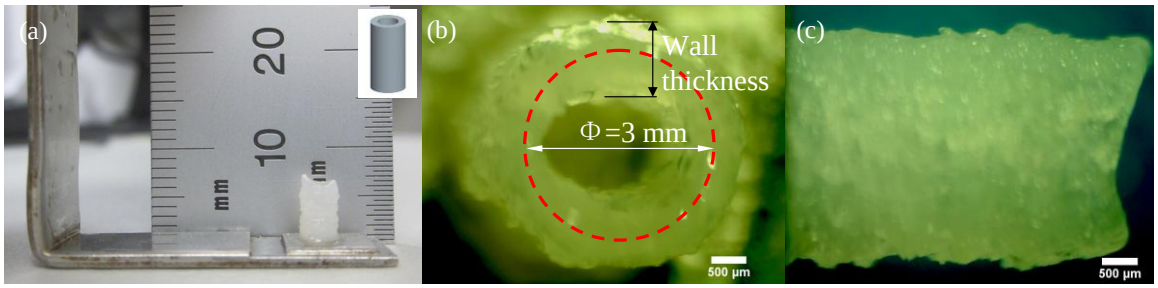

Fig. 5.1 (a) A representative tube fabricated using the proposed laser printing technique, (b) top view of the tube, and (c) side view of the tube

The entire process of laser-assisted printing can be divided into three steps: bubble formation, jet formation/breakup and jet/droplet landing. It should be noted that during laser-assisted direct writing such as LIFT, the material transfer and deposition can be due to either formed droplets [Barron2005] [Young2002] or the contact between formed long, thin jet and the receiving substrate [Duocastella2008] [Serra2009] depending on the direct writing height and material properties. In this study, the constructs were fabricated mostly due to the contact of alginate jets based on the imaging study of the printing process. Upon landing, both mechanical impact/spreading and chemical gelation happen simultaneously.

The jet formation process during laser printing of alginate solution can be classified into four different scenarios as shown in Fig. 5.2 depending on the laser fluence and the NaAlg concentration. During the printing process, once the energy of incident laser pulse is absorbed by the NaAlg solution-based ribbon coating, a high pressure, high

temperature bubble might form and further expand within the coating due to sublimation pressure [Lin2009b] [Guillemot2010b] [Wang2009]. Fully developed jets only form under certain operating conditions for a given NaAlg solution. If the laser fluence is too low and/or the NaAlg concentration is too high, which means a more viscous fluid, it is difficult for a bubble to fully form and/or expand before it diminishes [Lin2008]. As a result, jet may not fully form and further develop (Fig. 5.2(a)) since there is no enough kinetic energy provided by the expanding bubble. Instead, jet, if formed, retracts back after the bubble diminishes. If the laser fluence is too high and/or the NaAlg concentration is too low, it is also difficult to form a well developed jet as desired. Rapid, powerful bubble expansion may lead to a bulged shape [Unger2011] and even splashing [Lin2009b] [Duocastella2009a] as shown in Fig. 5.2(c) and (d), which is not ideal for pattern and construct printing. Only with some combinations of laser fluence and NaAlg concentration, jet can be fully developed as shown in Fig. 5.2(b). The laser fluence determines the jet kinetic energy, and the NaAlg concentration affects the viscous dissipation energy and the surface tension force. When the jet kinetic energy is higher than that of viscous dissipation, a jet forms; when the surface tension effect dominates and leads to the Rayleigh instability, the jet breaks up, forming flying droplets. It should be noted that if the jet kinetic energy is too high, it may end up with a bulged jet or splashing, which is not good for good printing performance.

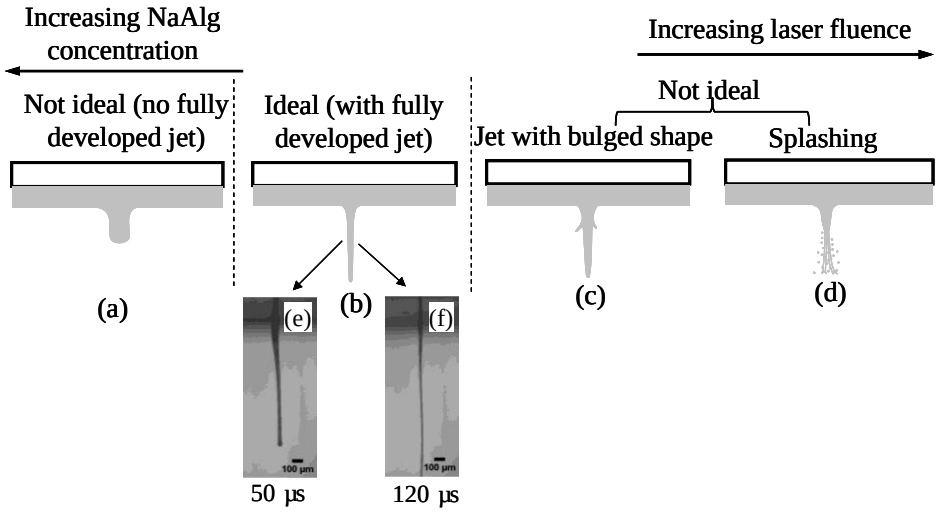

Fig. 5.2 Jet formation regimes and representative jet formation observations

To further illustrate the jet formation process, two representative jet observations are shown in Fig. 5.2(e) and (f) during the printing of 8% NaAlg solution under a laser fluence of 1183 ± 67 mJ/cm^2, taken at 50 μs and 120 μs, respectively. In this study, the jet fed alginate solution on the deposition location and broke up after deposition as reported in a previous study [Duocastella2010] instead of flying droplets. Both fluid properties and operating conditions affect the size of forming jets and the resolution of printed gel structure.

5.1.2 Effect of Sodium Alginate Concentration

To appreciate the effect of NaAlg concentration on the tube printing quality,

annular constructs (or short tubes) with a height of around 1 mm were printed from NaAlg solutions with different concentrations: 2%, 4%, 6% and 8%. Some of printed constructs are shown in Fig. 5.3(a) and (b) (150 μm laser spot size) and Fig. 5.3(c) and (d) (50 μm laser spot size) under a laser fluence of 1437 ± 28 mJ/cm^2. It can be seen that the printing quality increased with the increase of NaAlg concentration. As observed but not shown herein, the 1% NaAlg solution did not yield any good structure under all operating conditions investigated; only a bulky gel stack was obtained instead of a hollow cylindrical tube. Though annular constructs were formed using the 2% NaAlg solution, the construct quality was poor with a rough tube surface and non-uniform wall thickness as seen in Fig. 5.3(a) and (c). With the increase of NaAlg concentration, the tube surface became smoother, and the construct shape became better defined. Apparently, higher concentration NaAlg solutions (6% and 8%) yielded a better printing quality as seen in Fig. 5.3(b) and (d). The tube wall thickness and outer diameter are shown in Fig. 5.4 as the NaAlg concentration increases. In the following thickness and/or diameter plots (Figs. 22-24), the error bars represent the standard deviation (+/- one sigma) of the tube wall thickness and outer diameter. Herein the tube wall thicknesses were 0.89 mm, 0.86 mm, 0.78 mm, and 0.68 mm, respectively, showing a decreasing trend and the tube outer diameters were 3.55 mm, 3.52 mm, 3.41 mm and 3.35 mm, respectively, also showing a decreasing trend. The discrepancy between the laser spot size (150 μm in diameter) and

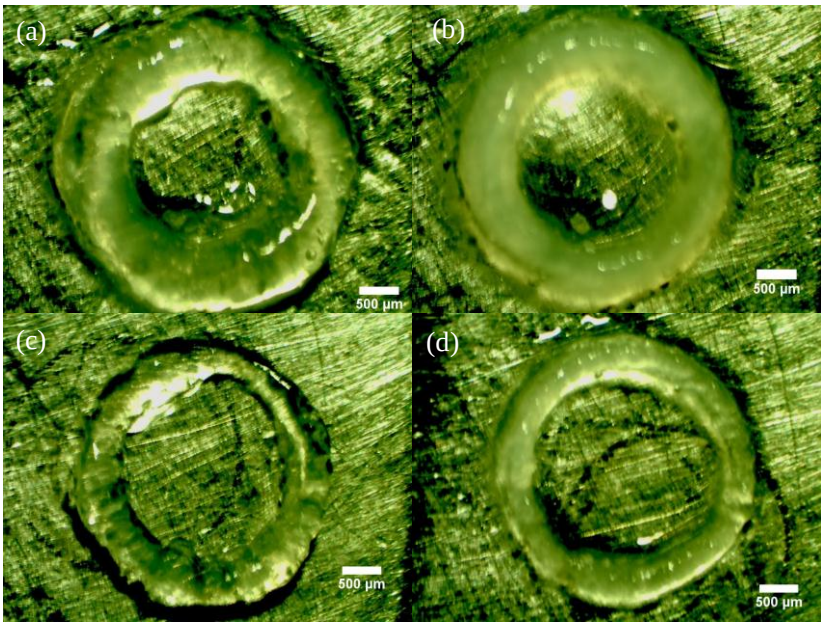

Fig. 5.3 Printed annular constructs/short tubes made from NaAlg solutions with different concentrations under a laser fluence of 1437 ± 28 mJ/cm^2: (a) 2%, (b) 8%, (c) 2% (50 µm laser spot size), and (d) 8% (50 µm laser spot size)

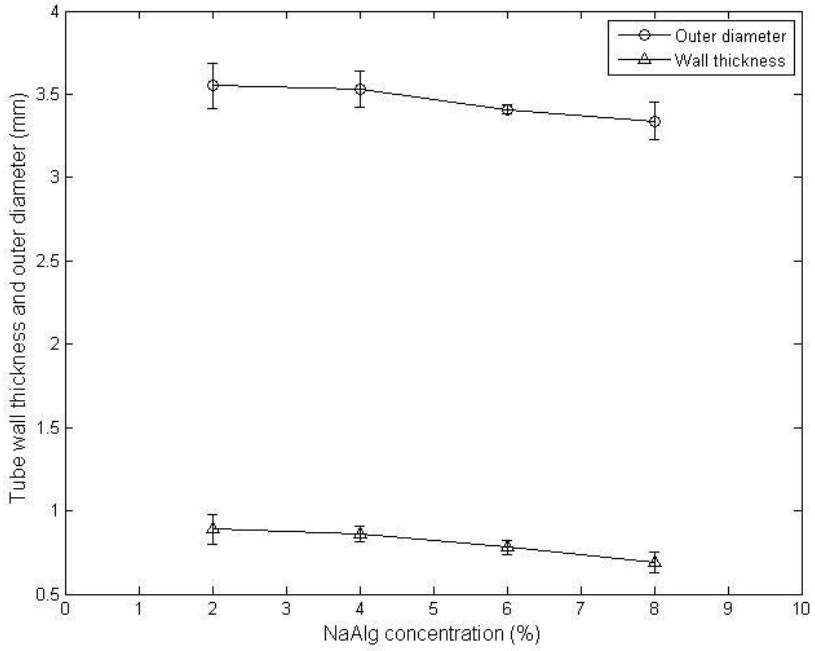

Fig. 5.4 Tube wall thickness and outer diameter as a function of NaAlg concentration (laser fluence 1437 ± 28 mJ/cm^2)

the resulted tube wall thickness (much larger than 150 μm) is attributed to the fluidic spreading of alginate jets when they landed on the previously deposited but gelatinized layer before their complete gelation.

A bubble may form upon the incidence of the laser pulse and eject the NaAlg solution beneath as a jet if the forming bubble provides enough kinetic energy. As the NaAlg concentration of the ribbon coating increases, the fluid viscosity increases significantly too. For example, the viscosity may increase almost twenty-seven times comparing those of 2% and 6% NaAlg solutions (94 ± 1 vs. 2618 ± 14 mPa s) [Lin2011]. A higher viscosity of the ribbon coating indicates a more pronounced viscous damping effect, resulting in a smaller ejection force for the transfer of alginate solution since more laser energy absorbed is consumed to overcome the viscous dissipation. As such, it leads to fewer materials being ejected and a slower jet if formed. Fewer materials ejected means a smaller-diameter jet/droplet per pulse with high concentration NaAlg solutions as observed in inkjetting NaAlg solution [Herran2012a]; in other words, a better printing resolution. Since the resolution of printed pattern is also affected by the landing velocity of jet/droplet, a lower velocity is expected to minimize the spreading effect, which can be accomplished using a high concentration solution. In addition, a viscous NaAlg jet/droplet is difficult to be spread upon landing, helping improve the printing resolution. On the other hand, a less viscous NaAlg solution is also likely to have a bulged shape or

induce splashing as shown in Fig. 5.2(c) and (d), deteriorating the printing quality. The effect of NaAlg concentration on the printing quality showed a similar trend under other laser fluences (1149 $\pm$34, 1698 $\pm$45, 2009 $\pm$45, and 2286 $\pm$45 mJ/cm^2). As discussed, a higher concentration alginate solution generally leads to a better printing resolution due to its higher viscosity and the resulting lower jet/droplet velocity if a jet can be successfully formed.

5.1.3 Effect of Laser Fluence

To appreciate the effect of laser fluence on the tube printing quality, annular constructs were further printed under the laser fluence level from 1149 $\pm$ 34 mJ/cm^2 to 2286 $\pm$45 mJ/cm^2. There were no monotonic trends for both the wall thickness (Fig. 5.5) and diameter as the laser fluence varied while the 1698 $\pm$ 45 mJ/cm^2 laser fluence resulted in the smaller wall thickness and tube diameter. The wall thickness and diameter increased first, then decrease, and finally increased as the laser fluence increased. For the 2% NaAlg solution, it was difficult to print a tubular structure under higher laser fluences (higher than 2009 $\pm$45 mJ/cm^2), so the related results were not reported in Fig. 5.5.

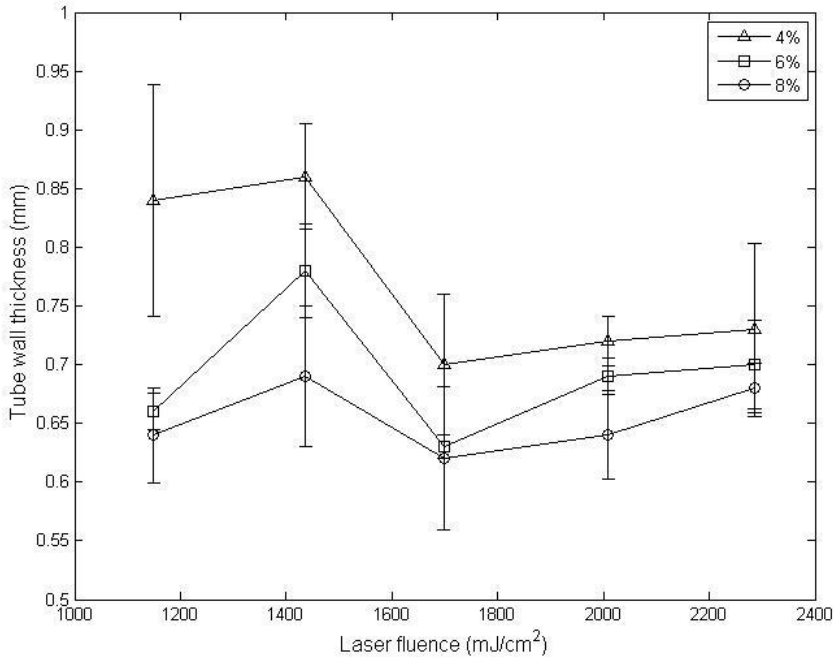

Fig. 5.5 Tube wall thickness as a function of laser fluence

When the laser fluence increases, it may lead to the following phenomena: 1) more materials transferred per pulse, 2) a higher speed jet/droplet or a higher landing velocity, 3) a well-developed jet with a smaller diameter within a certain fluence range as shown in Fig. 5.2(e) and (f), and 4) bulged or splashing jet when the laser fluence is too high. While the third result may lead to a better resolution, and the others may deteriorate the resolution. These results are kind of these competing factors in determining the pattern resolution herein. When the laser fluence is relatively low, the first and second phenomena dominate, resulting in an increasing wall thickness as observed. When the laser fluence is relatively high, the fourth result dominates, also resulting in an increasing

wall thickness as observed. Such an increasing trend as the external stimulation (such as the driving voltage in inkjetting) increases is also very common in inkjetting [Herran2012a] [Herran2010]. When the laser fluence is right to induce a well-developed jet, the stretching effect under a high inertia force may dominate and lead to a smaller wall thickness. As discussed, the printing quality has no monotonic trend as observed, and the exact relationship should be elucidated by studying the fluid dynamics of this printing process in a future study.

Overall, the printing quality is influenced by the fluid properties, and this influence is further illustrated in Fig. 5.6 as the NaAlg concentration and laser fluence change. Generally, the tube wall thickness and tube outer diameter decrease with the NaAlg concentration, while they first increase, then decrease and finally increase again with the laser fluence. The tube wall thickness and outer diameter are more sensitive to the change of NaAlg concentration under lower laser fluences. Similarly, the tube wall thickness and outer diameter are more sensitive to the change of laser fluence when using lower concentration NaAlg solutions. In other words, the NaAlg concentration dominates if the laser fluence is low, and the laser fluence dominates if the NaAlg concentration is low.

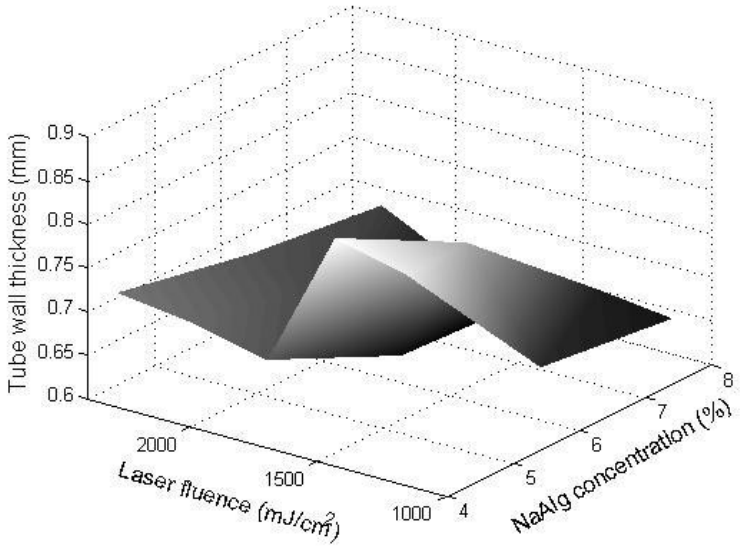

Fig. 5.6 Tube wall thickness as functions of laser fluence and NaAlg concentration

5.1.4 Effect of Laser Spot Size

Intuitively, the feature size should be reduced by using a smaller laser spot size. The effect of spot size on the printing quality has also been examined, and the results are shown in Fig. 5.7 when two different spot sizes (150 μm vs. 50 μm in diameter) were tested. Under the same laser fluence, the incident energy decreased as the spot size was smaller. As expected, both the tube wall thickness and outer diameter reduced as the laser spot size decreased since fewer materials were transferred per pass. However, it can be seen that the thickness did not reduced to one third as the spot size reduced to one third (from 150 μm to 50 μm) and the thickness reduction was more pronounced at higher laser fluences. This observation is attributed to the following reason. The spreading effect after

landing may be the dominating effect on the printing quality, overshadowing that of the jet/droplet size. On the other hand, this spreading effect is less significant when the jet/droplet is more viscous as with high concentration NaAlg solutions.

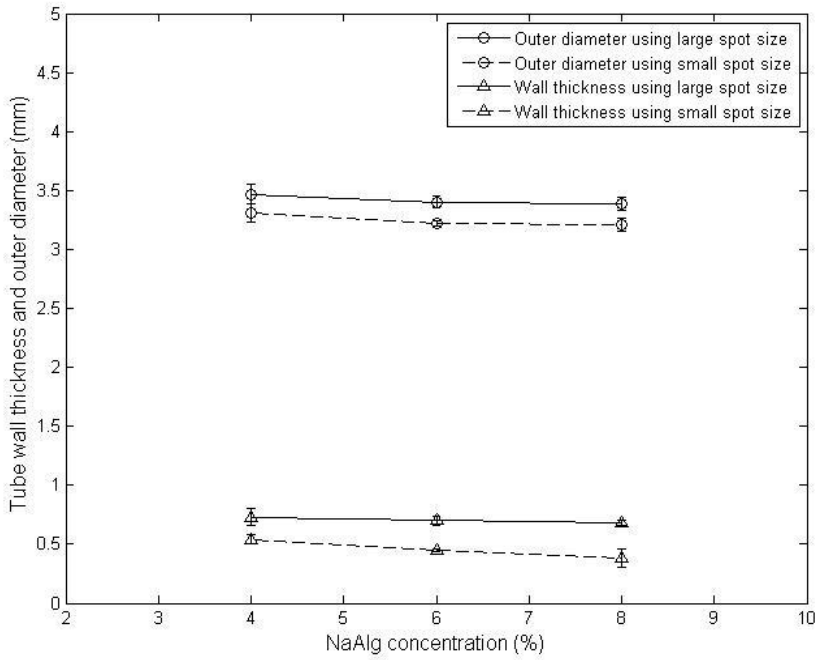

Fig. 5.7 Tube outer diameter and wall thickness under different spot sizes with a laser fluence of 2286 $\pm$ 45 mJ/cm^2

Varying the laser spot size demonstrates the possibility to improve the printing quality; however, there are some concerns with this approach. First, the printing productivity may decrease since each deposited layer is thinner, and more layers are needed for a given construct. Second, a higher laser fluence might be needed for effective transfer since the energy per pulse is the product of laser fluence and laser spot size.

Higher laser fluences may lead to more cell damage [Lin2009a] [Lin2010] during the printing of cellular constructs. In addition, slim constructs may buckle or collapse, so sometimes it is expected to use a relatively larger spot size to have a thick structure.

5.2 Laser-Assisted Printing of Cellular Tubes

Fig. 5.8 shows a representative cellular tube printed using the proposed laser printing technique, and the height of the tube is about 5 mm. The tube was printed using the prepared bioink under the laser fluence of 1026 ± 27 mJ/cm^2. The tube was made with 270 layers with the outer diameter of about 3 mm. Similar with alginate tube printing, the wall surface is rough and the tube top layer is not flat, which might be due to the pulse instability of the excimer laser and/or the spreading of deposited droplets during landing. What need to be mention about printing automation is that the liquid inside the tube was never pipetted out during the printing process. This can be a deficiency that needs to be solved in the future because the inner liquid (calcium chloride) may further gel the printed jet that lands inside the hole of the tube, making the tube wall thickness larger.

The measured cell viability immediately after printing was 65%, and the one after 24 hours of incubation was 80%, considering the control effect for both. Cells may die due to various reasons and the main reasons may include: 1) normal and shear stresses and thermo effects in printing process; 2) ion diffusion such that calcium ions in calcium

chloride may diffusion through the gel layer and further broke the ion balance of cells; 3) lack of nutrient during printing, since the in-printing structure may stay under liquid level for several minutes. After 24 hours of incubation, cells underwent recovery by self-repair or proliferation [Lin2009a]. However, much higher post-printing cell viability is needed in future studies.

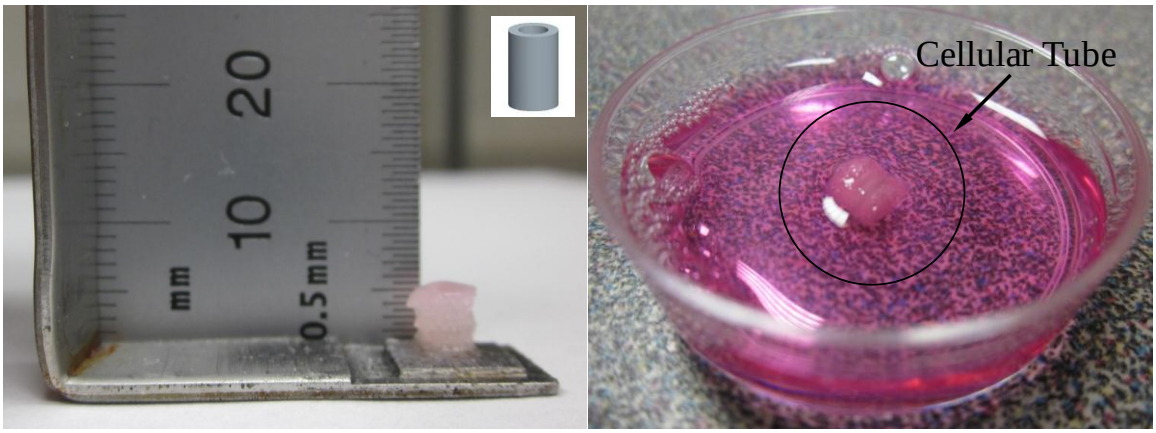

(a) (b)

Fig. 5.8 Representative cellular tubes fabricated by LIFT-based printing: (a) measurement of printed tube, and (b) printed tube for incubation

5.3 Conclusions

Laser-assisted printing such as LIFT has been well studied to pattern or fabricate 2D constructs while there is no investigation on its 3D printing performance. This study has investigated the effects of NaAlg concentration and operating conditions such as the laser fluence and laser spot size on the printing quality during laser-assisted printing of

alginate tubes with a nominal diameter of 3 mm. It is found that highly viscous materials can be printed into well-defined tubular constructs. As discussed, the printing quality is affected by the fluid properties and operating conditions. The tube wall thickness and tube outer diameter decrease with the NaAlg concentration, while first increasing, then decreasing and finally increasing again with the laser fluence. The NaAlg concentration dominates if the laser fluence is low, and the laser fluence dominates if the NaAlg concentration is low. Moreover, cellular tubes have been printing using the proposed laser-assisted printing technique. The immediate post-printing cell viability was 65%, while the one after 24 hours of incubation was 80%.

CHAPTER SIX

CONCLUSIONS AND FUTURE WORK

6.1 Conclusions

This thesis studies the laser-assisted direct writing of biomaterials and biological materials. The printing mechanism and process is studied by imaging analysis of laser-assisted printing two different fluids. The application of laser-assisted printing is further investigated by printing annular and tubular structures using both NaAlg and cell suspension. The major conclusions of this thesis are discussed as follows.

6.1.1 Laser-Assisted Printing of Glycerol

This study has investigated the effects of fluid properties as well as the combined effects of laser fluence and fluid properties on the jet formation process during laser-assisted direct writing of glycerol solutions. A time resolved imaging analysis-based approach has been implemented to investigate the jet formation process. It is found that the jetting dynamics is a function of fluid properties such as the glycerol concentration and operating conditions such as the laser fluence. If the laser fluence is too low and/or the glycerol concentration is too high, it is less likely for a bubble to fully form and/or

grow before it diminishes. There is no enough kinetic energy provided by the expanding bubble. Even when a jet can be formed, it retracts back after the bubble diminishes. If the laser fluence is too high and/or the glycerol concentration is too low, it is also difficult to form a well-developed jet since dramatic bubble expansion may lead to a bulgy shape and even splashing. Only under some selected conditions of glycerol concentration and laser fluence, can a well-defined jet form. When a jetting fluid is given, its jettability (J) can be characterized as the inverse of Ohnesorge number. It is observed that a good jet forms at $0.86 \leq J \leq 2.49$ in this study under the laser fluence of 717 ± 45 mJ/cm^2. To better appreciate the jettability, a phase diagram is expected by considering the contributions from both the material properties and the operating conditions in future studies.

6.1.2 Laser-Assisted Printing of Sodium Alginate

Laser-assisted printing of both viscoelastic and Newtonian fluids are investigated in this study in order to better understand the printing mechanism. Time-resolved imaging analysis is carried to study the effect of fluid properties and operating conditions including laser fluence, laser spot size and direct writing height in terms of the jet development process and jet morphology. It is found that the jetting dynamics is functions of both material properties and operating conditions. Both Ohnesorge number and Deborah number increase while Reynolds number decreases with NaAlg

concentration. As of laser fluence, only Reynolds number is influenced and it increases with the laser fluence. An operating diagram relating Deborah number and Reynolds number is constructed for dividing the different printing regimes: jet contact-based printing, droplet contact-based printing and no deposition. BOAS phenomenon has been observed in different cases in this study. It is demonstrated that BOAS phenomena can be only observed under higher laser fluences and higher concentration NaAlg solutions.

6.1.3 Laser-Assisted Printing of Structures

Laser-assisted printing such as LIFT has been well studied to pattern or fabricate 2D constructs while there is no investigation on its 3D printing performance. This study has investigated the effects of NaAlg concentration and operating conditions such as the laser fluence and laser spot size on the printing quality during laser-assisted printing of alginate tubes with a nominal diameter of 3 mm. It is found that highly viscous materials can be printed into well-defined tubular constructs. As discussed, the printing quality is affected by the fluid properties and operating conditions. The tube wall thickness and tube outer diameter decrease with the NaAlg concentration, while first increasing, then decreasing and finally increasing again with the laser fluence. The NaAlg concentration dominates if the laser fluence is low, and the laser fluence dominates if the NaAlg concentration is low. Moreover, cellular tubes have been printing using the proposed

laser-assisted printing technique. The immediate post-printing cell viability was 65%, while the one after 24 hours of incubation was 80%.

6.2 Future Work

Though inkjet printing and laser-assisted printing has been demonstrated potential use in cell and/or organ printing, it should be noted that the cellular tube printing is only the first step towards real application. Much work should be done in order to seek this technique's application in biomedical field.

6.2.1 Imaging Analysis of Laser-Assisted Printing

To better understand the different laser-assisted printing regimes, future study may include: (1) more detailed experimental and theoretical investigation on determining the relaxation time of different NaAlg solutions in order to calculate related dimensionless groups; (2) further understanding of the behavior of Newtonian and viscoelastic solutions in the printing process by combining theoretical and imaging studies; (3) more comprehensive and detailed operating diagrams that cover the effects of fluid properties and all the operating conditions on different printing regimes; and (4) an operation diagram regarding both viscoelastic and Newtonian fluid.

6.2.2 Laser-Assisted Printing of Structures

For better biofabrication and biomedical applications of laser-assisted printing technique, future work may include: (1) printing of longer tubes with smaller tube wall thickness using the proposed printing automation; (2) printing of more complex structures such as Y-shaped or zigzag-shaped tubes; (3) use of sacrificial layer(s) for process improvement; (4) printing of cellular tubes using high concentration cell suspension for mimicking the real tissue environment; (5) printing of multi-layered cellular tube using different cell types to mimic the real blood vessels; (6) demonstration cell fusion inside the printed cellular tubes; and (7) use of other biocompatible materials such as collagen and matrigel in cellular tube printing to try to get a higher post-printing cell viability. In addition, other organ printing-related topics might be of interest such as the maximum size of obtainable biological constructs, the behavior of the construct being built in the solution/container over a longer period of time, and the change of properties of the solution with the volume of the construct being built.

6.2.3 Modeling of Laser-Assisted Printing Process

The theoretical work regarding the LIFT-based printing is still currently lacking. Therefore, modeling the entire process of printing is needed. Future work may include: (1)

the modeling of bubble formation process, including laser-material interaction modeling; (2) modeling of jet formation process, including mathematical and software modeling; (3) modeling of the jet landing process, including mechanical modeling and chemical reaction modeling; and (4) the development of mathematical models accounting for the entire printing process including jet/droplet formation, landing, spreading, gelation, and even the cell damage process.

REFERENCES

[Barbulovic-Nad2006] Barbulovic-Nad, I., Lucente, M., Sun, Y., Zhang, M., Wheeler, A. R., and Bussmann, M., 2006, "Bio-microarray Fabrication Techniques - a Review," Critical Reviews in Biotechnology, Vol. 26(4), pp. 237-259.

[Barron2004] Barron, J. A., Ringeisen, B. R., Kim, H., Spargo, B. J., and Chrisey, D. B., 2004, "Application of Laser Printing to Mammalian Cells," Thin Solid Films, Vol. 453-454, pp. 383-387.

[Barron2005] Barron, J. A., Yong, H. D., Dlott, D. D., Darfler, M. M., Krizman, D. B., and Ringeisen, B. R., 2005, "Printing of Protein Microarrays via a Capillary-Free Fluid Jetting Mechanism," Proteomics, Vol. 5(16), pp. 4138-4144.

[Boland2006] Boland, T., Xu, T., Damon, B., and Cui, X., 2006, "Application of Inkjet Printing to Tissue Engineering," Biotechnol. J., Vol. 1(9), pp. 910-917.

[Boland2007] Boland, T., Xu, T., Damon, B. J., Manley, B., Kesari, P., Jalota, S., and Bhaduri, S., 2007, "Drop-on-Demand Printing of Cells and Materials for Designer Tissue Constructs," Mater. Sci. Eng. C, Vol. 27(3), pp. 372-376.

[Brown2010] Brown, M. S., Kattamis, N, T., and Arnold, C. B., 2010, "Time-Resolved Study of Polyimide Absorption Layers for Blister-Actuated Laser-Induced Forward Transfer," J. Appl. Phys. Vol. 107(8), pp. 083103(1-8).

[Brown2011] Brown, M. S., Kattamis, N. T., and Arnold, C. B., 2011, "Time-Resolved Dynamics of Laser-Induced Micro-jets from Thin Liquid Films," Microfluid Nanofluid, Vol. 11(2), pp. 199-207.

[Brujan2005] Brujan, E. A., Ikeda, T., and Matsumoto, Y., 2005, "Jet Formation and Shock Wave Emission during Collapse of Ultrasound-Induced Cavitation Bubbles and Their Role in the Therapeutic Applications of High-Intensity Focused Ultrasound," Phys. Med. Biol., Vol. 50(20), pp. 4797-4809.

[Brujan2006] Brujan, E. A., and Vogel, A., 2006, "Stress Wave Emission and Cavitation Bubble Dynamics by Nanosecond Optical Breakdown in a Tissue Phantom," J. Fluid Mech., Vol. 558(1), pp. 281-308.

[Catros2011] Catros, S., Fricain, J., Guillotin, B., Pippenger, B., Bareille, R., Remy, M., Lebraud, E., Desbat, B., Amédée, J., and Guillemot, F., 2011, "Laser-Assisted Bioprinting for Creating on-Demand Patterns of Human Osteoprogenitor Cells and Nano-hydroxyapatite," Biofabrication, Vol. 3(2), pp. 025001(1-11).

[Clasen2011] Clasen, C., Phillips, P. M., Palangetic, L., and Vermant, J., 2011, "Dispensing of Rheologically Complex Fluids: The Map of Misery," AIChE Journal, Vol. 58(10), pp. 3242-3255.

[Colina2006] Colina, M., Duocastella, M., Fernandez-Pradas, J. M., and Morenza, J. L., 2006, "Laser-Assisted Forward Transfer of Liquids: Study of the Droplet Ejection Process," J. Appl. Phys. Vol. 99(8), pp. 084909(1-7).

[Cooper-White2002] Cooper-White, J. J., Fagan, J. E., Tirtaatmadja, V., Lester, D. R., and Boger, D. V., 2002, "Drop Formation Dynamics of Constant Low-Viscosity, Elastic Fluids," J. Non-Newtonian Fluid Mech., Vol. 106(1), pp. 29-59.

[Duocastella2007] Duocastella, M., Colina, M., Fernandez-Pradas, J. M., Serra, P., and Morenza, J. L., 2007, "Study of the Laser-Induced Forward Transfer of Liquids for Laser Bioprinting," Appl. Surf. Sci., Vol. 253(19), pp. 7855-7859.

[Duocastella2008] Duocastella, M., Fernandez-Pradas, J. M., Serra, P., and Morenza, J. L., 2008, "Jet Formation in the Laser Forward Transfer of Liquids," Appl. Phys. A., Vol. 93(2), pp. 453-456.

[Duocastella2009] Duocastella, M., Fernández-Pradas, J. M., Morenza, J. L., and Serra, P., 2009, "Time-Resolved Imaging of the Laser Forward Transfer of Lquids," J. Appl. Phys., Vol. 106(8), pp. 084907(1-7).

[Duocastella2010] Duocastella, M., Fernández-Pradas, J. M., Morenza, J. L., and Serra, P., 2010, "Sessile Droplet Formation in the Laser-Induced Forward Transfer of Liquids: a Time-Resolved Imaging Study," Solid Thin Films, Vol. 518(18), pp. 5321-5325.

[Duocastella2011a] Duocastella, M., Patrasciois, A., Dinca, V., Fernández-Pradas, J. M., Morenza, J. L., and Serra, P., 2011, "Study of Liquid Deposition During Laser Printing of Liquids," Appl. Surf. Sci., Vol. 257(12), pp. 5255-5258.

[Duocastella2011b] Duocastella, M., Fernández-Pradas, J. M., Morenza, J. L., and Serra, P., 2011, "Droplet Printing Through Bubble Contact in the Laser Forward Transfer of Liquids," Appl. Surf. Sci., Vol. 257(7), pp. 2825-2829.

[Fabbro1990] Fabbro, R., Fournier, J., Ballard, P., Devaux, D., and Virmont, J., 1990, "Physical Study of Laser-produced Plasma in Confined Geometry," J. Appl. Phys., Vol. 68(2), pp.775-784.

[Graessley1980] Graessley, W. W., 1980, "Polymer Chain Dimensions and the Dependence of Viscoelastic Properties on Concentration, Molecular Weight and Solvent Power," Polymer, Vol. 21(3), pp. 258-262.

[Gruene2011] Gruene, M., Deiwick, A., Koch, L., Schlie, S., Unger, C., Hofmann, N., Bernemann, I., Glasmacher, B., and Chichkov, B., 2011, "Laser Printing of Stem Cells for Biofabrication of Scaffold-Free Autologous Grafts," Tissue Eng. C, Vol. 17(1), pp. 79-87.

[Guilemot2010a] Guillemot, F., Souquet, A., Catros, S., Guillotin, B., Lopez, J., Faucon, M., Pipenger, B., Bareille, R., Rémy, M., Bellance, S., Chabassier, P., Fricain, J. C., and Amédée, J., 2010, "High-throughput Laser Printing of Cells and Biomaterials for Tissue Engineering," Acta Biomaterialia, Vol. 6(7), 2494-2500.

[Guillemot2010b] Guillemot, F., Souquet, A., Catros, S. and Guillotin, B., 2010, "Laser-Assisted Cell Printing: Principle, Physical Parameters versus Cell Fate and Perspectives in Tissue Engineering," Nanomedicine, Vol. 5(3), pp. 507-515.

[Herren2010] Herran, C. L., Wang, W., Huang, Y., Mironov, V., and Markwald, R., 2010, "Parametric Study of Acoustic Excitation-Based Glycerol-Water Microsphere Fabrication in Single Nozzle Jetting," J. Manuf. Sci. Eng. E-T ASME, Vol. 132, pp. 051001 (1-7).

[Herran2012a] Herran, C. L., and Huang, Y., 2012, "Alginate Microsphere Fabrication Using Bipolar Wave-Based Drop-on-Demand Jetting," Journal of Manufacturing Processes, Vol. 14(2), pp. 98-106.

[Herran2012b] Herran, C. L., Huang, Y., and Chai, W., 2012, "Performance Evaluation of Bipolar and Tripolar Excitations during Nozzle-Jetting-Based Alginate Microsphere Fabrication," J. Micromech. Microeng., Vol. 22(8), pp. 085025(1-11).

[Jang2009] Jang, D., Kim, D., and Moon, J., 2009, "Influence of Fluid Physical Properties on Inke-Jet Printability," Langmuir, Vol. 25(5), pp. 2629-2635.

[Kattamis2007] Kattamis, N. T., Purnick, P. E., Weiss, R., and Arnold, C. B., 2007, "Thick Film Laser Induced Forward Transfer for Deposition of Thermally and Mechanically Sensitive Materials," Appl. Phys. Lett., Vol. 91(17), pp. 171120.

[Kaur2009] K. S. Kaur, R. Fardel, T. C. May-Smith, M. Nagel, D. P. Banks, C. Grivas, T. Lippert, and R. W. Eason, 2009, "Shadowgraphic Studies of Triazene Assisted Laser-Induced Forward Transfer of Ceramic Thin Films," J. Appl. Phys. Vol. 105(11), pp. 113119(1-8).

[Khalil2005] Khalil, S., Nam, F., and Sun, W., 2005, "Multi-nozzle Deposition for Construction of 3D Biopolymer Tissue Scaffolds," Rapid prototyping J., Vol. 11(1), pp. 9-17.

[Koch2010] Koch, L., Kuhn, S., Sorg, H., Gruene, M., Schlie, S., Gaebel, R., Polchow, B., Reimers, K., Stoelting, S., Ma, N., Vogt, P. M., Steinhoff, G., and Chinchkov, B., 2010, "Laser Printing of Skin Cells and Human Stem Cells," Tissue Eng. C, Vol. 16(5), pp. 847-854.

[Koch2012] Koch L, Deiwick, A., Schlie, S., Michael, S., Gruene, M., Vincent, C., Zychlinski, D., Schambach, A., Reimers, K., Vogt, P. M., and Chichkov, B., 2012, "Skin Tissue Generation by Laser Cell Printing," Biotechnol. Bioeng., Vol. 109(7), pp. 1855-1863.

[Lauterborn1997] Lauterborn, W., and Ohl, C., 1997, "Cavitation Bubble Dynamics," Ultrasonics Sonochemistry, Vol. 4(2), pp. 65-75.

[Lewis2004] Lewis, J. A., and Gratson, G. M., 2004, "Direct Writing in Three Dimensions," Materials Today, Vol. 7(7-8), pp. 32- 39.

[Lin2008] Lin, Y., Foy, K., Huang, Y., and Chrisey, D. B., 2008, "Bubble Formation Modeling in Matrix-Assisted Pulsed-Laser Evaporation Direct Write," Proc. of the 2008 ASME International Manufacturing Science and Engineering Conference (MSEC 2008), Evanston, Illinois, USA, MSEC_ICMP2008-72241 1-8.

[Lin2009a] Lin, Y., Huang, Y., Wang, G., Tzeng, T. J., and Chrisey, D. B., 2009, "Effect of Laser Fluence on Yeast Cell Viability in Laser-Assisted Cell Transfer," J. Appl. Phys., Vol. 106(4), pp. 043106(1-7).

[Lin2009b] Lin, Y., Huang, Y. and Chrisey, D. B., 2009, "Droplet Formation in Matrix-Assisted Pulsed-Laser Evaporation Direct Writing of Glycerol-Water Solution," J. Appl. Phys., Vol. 105(9), pp. 093111(1-6).

[Lin2010] Lin, Y., Huang, G., Huang, Y., Tzeng, T. J., and Chrisey, D. B., 2010, "Effect of Laser Fluence in Laser-Assisted Direct Writing of Human Colon Cancer Cell," Rapid Prototyping J., Vol. 16(3), pp. 202-208.

[Lin2011] Lin, Y., and Huang, Y., 2011, "Laser-Assisted Fabrication of Highly Viscous Alginate Microsphere," J. Appl. Phys., Vol. 109(8), pp. 083107(1-8).

[McKinley2011] McKinley, G. H., and Renardy, M., 2011, "Wolfgang von Ohnesorge," Phys. Fluids, Vol. 23(12), pp. 127101(1-6).

[Mironov2003] Mironov, V., Boland, T., Trusk, T., Forgacs, G., and Markwald, R. R., 2003, "Organ Printing: Computer-Aided Jet Contact-Based 3D Tissue Engineering," Trends Biotechnol., Vol. 21(4), pp. 157-161.

[Mironov2009] Mironov, V., Visconti, R. P., Kasyanov, V., Forgacs, G., Drake, C. J., and Markwald, R. R., 2009, "Organ Printing: Tissue Spheroids as Building Blocks," Biomaterials, Vol. 30(12), pp. 2164-2174.

[Morrison2010] Morrison, N. F. and Harlen, O. G., 2010, "Viscoelasticity in Inkjet Printing," Rheol Acta, Vol. 49(6), pp. 619-632.

[Nishiyama2009] Nishiyama, Y., Nakamura, M., Henmi, C., Yamaguchi, K., Mochizuki, S., Nakagawa, H., and Takiura, K., 2009, "Development of a Three-Dimensional Bioprinter: Construction of Cell Supporting Structures Using Hydrogel and State-of-the-Art Inkjet Technology," J. Biomech. Eng., Vol. 131(3), pp. 035001(1-6).

[Norman2006] Norman, J. J., and Desai, T. A., 2006, "Methods for Fabrication of Nanoscale Topography for Tissue Engineering Scaffolds," Ann. Biomed. Eng., Vol. 34(1), pp. 89-101.

[Park1994] Park, H. K., 1994, "Heat and Momentum Transfer on the Rapid Phase Change of Liquid Induced by Nanosecond-Pulsed Laser Irradiation," University of California, Berkeley, Ph. D. Dissertation.

[Phamduy2012] Phamduy, T. B., Raof, N. A., Schiele, N. R., Yan, Z., Corr, D. T., Huang, Y., Xie, Yubing, and Chrisey, D. B., 2012, "Laser Direct-Write of Single Microbeads into Spatially-Ordered Patterns," Biofabrication, Vol. 4(2), pp. 025006(1-12).

[Riggs2011] Riggs, B. C., Dias, A. D., Schiele, N. R., Cristescu, R., Huang, Y., Corr, D. T., and Chrisey, D. B., 2011, "Matrix-Assisted Pulsed Laser Methods for Biofabrication," MRS Bulletin, Vol. 36(12), pp. 1043-1050.

[Ringeisen2004] Ringeisen, B. R., Kun, H., Barron, J. A., Krizman, D. B., Chrisey, D. B., Jackman, S., Auyeung, R. Y. C., and Spargo, B. J., 2004, "Laser Printing of Pluripotent Embryonal Carcinoma Cells," Tissue Eng., Vol. 10(3-4), pp. 483-491.

[Ringeisen2006] Ringeisen, B. R., Othon, C. M., Barron, J. A., Yong, D., and Spargo, B. J., 2006, "Jet-Based Methods to Printing Living Cells," Biotech. J., Vol. 1(9), pp. 930-948.

[Schaffer2002] Schaffer, C. B., Nishimura, N., Glezer, E. N., Kim, A. M. T., and Mazur, E., 2002, "Dynamics of Femtosecond Laser-Induced Breakdown in Water From Femtosecond to Microseconds," Opt. Express, Vol. 10(3), pp. 196-203.

[Schiele2010] Schiele, N. R., Corr, D. T., Huang, Y., Raof, N. A., Xie, Y., and Chrisey, D. B., 2010, "Laser-Based Direct-Write Techniques for Cell Printing," Biofabrication, Vol. 2(3), pp. 032001(1-14).

[Serra2009] Serra, P., Duocastella, M., Fernández-Pradas, J. M., and Morenza, J. L., 2009, "Liquids Microprinting Through Laser-Induced Forward Transfer," Appl. Surf. Sci., Vol. 255(10), pp. 5342-5345.

[Sollier2001] Sollier, A., Berthe, L., and Fabbro, R., 2001, "Numerical Modeling of the Transmission of Breakdown Plasma Generated in Water during Laser Shock Processing," Eur. Phys. J. Appl. Phys., Vol. 16(2), pp. 131-139.

[Tan2007] Tan, W. H. and Takeuchi, S., 2007, "Monodisperse Alginate Hydrogel Microbeads for Cell Encapsulation," Adv. Mater., Vol. 19 (18), 2696-2701.

[Tirtaatmadja2006] Tirtaatmadja, V., McKinley, G. H., and Cooper-White, J. J., 2006, "Drop Formation and Breakup of Low Viscosity Elastic Fluids: Effects of Molecular Weight and Concentration," Physics of Fluids, Vol. 18(4), pp. 043101(1-67).

[Unger2011] Unger, C., Gruene, M., Koch, L., Koch, J., and Chichkov, B., 2011, "Time-Resolved Imaging of Hydrogel Printing via Laser-Induced Forward Transfer," Appl. Phys. A, Vol. 103(2), pp. 271-277.

[Vogel2003] Vogel, A., and Venugopalan, V., 2003, "Mechanisms of Pulsed Laser Ablation of Biological Tissues," Chemical Review, Vol. 103(2), pp. 577-644.

[Vogel2007] Vogel, A., Lorenz, K., Horneffer,V., Hüttmann, G., von Smolinski, D., and Gebert, A., 2007, "Mechanisms of Laser-induced Dissection and Transport of Histologic Specimens," Biophysical Journal, Vol. 93(12), pp. 4481-4500.

[Vold2006] Vold, I. M., Kristiansen, K. A., and Christensen, B. E., 2006, "A Study of the Chain Stiffness and Extension of Alginates, in Vitro Epimerized Alginates, and Periodate-Oxidized Alginates Using Size-Exclusion Chromatography Combined with Light Scattering and Viscosity Detectors," Biomacromolecules, Vol. 7(7), pp. 2136-2146.

[Wang2009] Wang, W., Li, G., and Huang, Y., 2009, "Modeling of Bubble Expansion-Induced Cell Mechanical Profile in Laser-Assisted Cell Direct Writing," J. Manuf. Sci. E-T ASME, Vol. 131(5), pp. 051013(1-10).

[Wang2011] Wang, W., Lin, Y., and Huang, Y., "Modeling of Thermoelastic Stress Wave in Laser-Assisted Cell Direct Writing," ASME J. of Manufacturing Sci. and Eng., Vol. 133(2), pp. 024502(1-6).

[Wilson2003] Wilson, W. C., and Boland, T., 2003, "Cell and Organ Printing 1: Protein and Cell Printers," Anat Rec A, Vol. 272A(2), pp. 491-496.

[Wohlers2001] Wohlers, T., 2001, "Wohlers Report 2001: Rapid Prototyping and Tooling, State of the Industry," Annual Worldwide Progress Report, Wohlers Associates, Fort Collins, Colorado.

[Wu2001] Wu, P. K., Ringeisen, B. R., Callahan, J., Brooks, M., Bubb, D. M., Wu, H. D., Piqué, A., Spargo, B., McGill, R. A., and Chrisey, D. B., 2001, "The Deposition, Structure, Pattern Deposition, and Activity of Biomaterial Thin-Films by Mateix-Assisted Pulsed-Laser Evaporation (MAPLE DW) and MAPLE direct write," Thin Solid Films, Vol. 398-399, pp. 607-614.

[Wüst2011] Wüst, S., Müller, R., and Hofmann, S., 2011, "Controlled Positioning of Cells in Biomaterials - Approaches towards 3D Tissue Printing," J. Funct. Biomater, Vol. 2(3), pp. 119-154.

[Xu2012] Xu, C., Chai, W., Huang, Y., and Markwald, R. R., 2012, "Scaffold-Free Inkjet Printing of Three-Dimensional Zigzag Cellular Tubes," Biotechnol. Bioeng., Vol. 109(12), pp. 3152-3160.

[Yan2011] Yan, X., Carr, W. W., and Dong, H., 2011, "Drop-on-Demand Drop Formation of Polyethylene Oxide Solutions," Physics of Fluids, Vol. 23(10), pp. 107101(1-15).

[Yan2012] Yan, J., Huang, Y., Xu, C., and Chrisey, D. B., 2012, "Effects of Fluid Properties and Laser Fluence on Jet Formation during Laser Direct Writing of Glycerol Solutions," J. of Appl. Phys., Vol. 112(8), pp. 083105(1-8).

[Young2002] Young, D., Auyeung, R. C. Y., Piqué, A., Chrisey, D. B., and Dlott, D. D., 2002, "Plume and Jetting Regimes in a Laser Based Forward Transfer Process as Observed by Time-Resolved Optical Microscopy," Appl. Surf. Sci., Vol. 197-198, pp. 181-187.

[Yoo2001] Yoo, J. H., Borisov, O. V., Mao, X., and Russo, R. E., 2001, "Existence of Phase Explosion during Laser Ablation and Its Effects on Inductively Coupled Plasma-Mass Spectroscopy," Anal. Chem., Vol. 73(10), pp. 2288-2293.